Possibilities of Biomedical Application of Gadolinium Oxide Nanoparticles for Regenerative Medicine

Ekaterina V. Silina *, Natalia E. Manturova, Elena L. Chuvilina, Akhmedali A. Gasanov, Olga I. Andreeva, Maksim A. Pugachevskii, Aleksey V. Kochura, Alexey A. Kryukov, Yulia G. Suzdaltseva, and Victor A. Stupin

Posted Date: 19 November 2024

doi: 10.20944/preprints202411.1441.v1

Keywords: nanoparticles; gadolinium oxide; nanomaterials; nanogadolinium; regeneration; biomedicine; cytotoxicity; drug development

Article

Possibilities of Biomedical Application of Gadolinium Oxide Nanoparticles for Regenerative Medicine

Ekaterina V. Silina [1,*,†], Natalia E. Manturova [2], Elena L. Chuvilina [3], Akhmedali A. Gasanov [3], Olga I. Andreeva [3], Maksim A. Pugachevskii [4], Aleksey V. Kochura [4], Alexey A. Kryukov [5], Yulia G. Suzdaltseva [6] and Victor A. Stupin [2,†]

[1] I.M. Sechenov First Moscow State Medical University (Sechenov University), 119991 Moscow, Russia
[2] Pirogov Russian National Research Medical University (RNRMU), 117997 Moscow, Russia
[3] "LANHIT" LLC, 105118 Moscow, Russia
[4] Southwest State University, 50 let Oktyabrya Str., 94, 305040 Kursk, Russia
[5] Kursk State Medical University, Karl Marx Str., 3, 305041 Kursk, Russia
[6] Vavilov Institute of General Genetics, Russian Academy of Sciences, Gubkin Str., 3, Moscow 119333, Russia
* Correspondence: silinaekaterina@mail.ru
† These authors contributed equally to this work.

Abstract: Background/Objectives: The aim is to study the possibilities of biomedical application of gadolinium oxide nanoparticles (Gd_2O_3 NPs) synthesized under industrial conditions, evaluating its physicochemical properties, redox activity, biological activity and safety towards different human cell lines. **Methods:** The powderofGd_2O_3 NPs was studied using transmission electron microscopy (TEM), X-Ray Diffraction (XRD), Raman spectroscopy, mass spectrometry, scanning electron microscopy (SEM) with energy dispersive X-ray analyzer (EDX). The redox activity of different concentrations of Gd_2O_3 NPs was studied by optical spectroscopy (OS) method in the photochemical degradation process of methylene blue dye upon irradiation with optical source. Biological activity was studied on different human cell lines (keratinocytes, fibroblasts, mesenchymal stem cells (MSCs)) with evaluation of the effect of a wide range of Gd_2O_3 NPs concentrations (10^{-2}- 10^{-6}M) on metabolic and proliferative cellular activity (MTT test, direct cell counting, dead cell assessment, visual assessment of cytoarchitectonics). On MSC culture, the test of migration activity assessment on a model wound was performed. **Results:** From TEM data, the size of the nanoparticles ranged from 2 nm to 45 nm with a maximum distribution of 20-25 nm, which was in agreement with other methods. XRD analysis revealed that the f Gd_2O_3 nanoparticles had a cubic structure (C-form) of f Gd_2O_3 ($Ia\overline{3}$) with lattice parameter a = 10.79(9) Å. Raman spectroscopy showed that the f Gd_2O_3 nanoparticles had a high degree of crystallinity. By investigating the photooxidative degradation of methylene blue dye in the presence of f Gd_2O_3 NPs under red light irradiation, it was found that f Gd_2O_3 nanoparticles showed weak antioxidant activity, which depended on the particle content in the solution. At a concentration of 10^{-3}M, the highest antioxidant activity of f Gd_2O_3 nanoparticles was observed when the reaction rate constant of dye photodegradation decreased by 5.5% to 9.4x10-3 min^{-1}. When the concentration of f Gd_2O_3 NPs in solution was increased to 10^{-2}M upon irradiation with a red light source, their antioxidant activity changed to pro-oxidant activity, accompanied by a 15% increase in the reaction rate of methylene blue degradation. Studies on cell lines showed a high level of safety and regenerative potential of Gd_2O_3 NPs, which stimulated fibroblast metabolism at concentrations of 10^{-2}M to 10^{-3}M (27% enhancement), stimulated keratinocyte metabolism at concentrations of 10^{-3}M-10^{-5}M, and enhanced keratinocyte proliferation by an average of 35% at concentrations of 10^{-4}M; accelerated the migration of MSCs, enhancing their proliferation, promoting the healing of the model wound. **Conclusions:** The results of the study demonstrated the safety and high regenerative potential of redox-active Gd_2O_3 NPs towards different cell lines. This may be the basis for further research to develop nanomaterials based on Gd_2O_3 NPs for skin wound healing and in regenerative medicine generally.

Keywords: nanoparticles; gadolinium oxide; nanomaterials; nanogadolinium; regeneration; biomedicine; cytotoxicity; drug development

 doi:10.20944/preprints202411.1441.v1

1. Introduction

Rapidly changing technologies in all areas of our lives are increasingly leading to the discovery and practical application of new knowledge. Over the last two decades, much attention has been paid to the specific effects of nanomaterials, often difficult to explain in terms of routine chemical, physical and biological concepts. This explosive growth of interest is well illustrated by the increasing number of publications in the scientific literature. But while much has already been achieved in technical applications, we are only at the beginning of the road when it comes to medical aspects. The reason for this is the potential toxicity of metal nanoparticles and the possibility of their unexpected penetration through cell membranes with unpredictable outcomes [1–5].

In 2006, the Medical Advisory Secretariat published a forecast on the development of nanotechnology in medicine and predicted that by 2024, nanotechnology solutions aimed at detection of DNA mutations and gene expression, creation of disease markers, drug delivery with controlled release, targeted tissue sequestration and thermal ablation of deep tumor tissues, multifunctional therapeutics with targeted drug delivery and penetration enhancers will be introduced into clinical practice [6]. If we talk about practical medical applications today, of all the goals set by the Medical Advisory Secretariat, perhaps only gadolinium nanoparticles chelated to prevent toxic effects have become widely used as a contrast agent in magnetic resonance imaging (MRI) [7–10]. After the first such drug (Magnevist) appeared on the medical market in the 1980s, it was gadolinium (Gd) in the form of Gd_2O_3 chelates and, more often, Gd_2 oxide that became widely used as a contrast agent for MRI, and today there are several tens of contrast agents based on Gd_2O_3 on the world market, due to its unique physical and chemical properties as well as high magnetic susceptibility of Gd^{3+} due to the presence of seven unpaired electrons (S = 7/2) at the 4f energy sublevel, which is extremely magnetic [11–13]. However, there are no other such successful examples in nanomedicine. This story well illustrates the difficulty of bringing any scientific project to practical application, especially in medicine, due to the supercomplexity of predicting the effects of nanoparticles or complexes including nanoparticles. However, judging by the number of publications in PubMed, the interest in nanotechnology in medicine has not only not weakened, but has increased manifold. According to PubMed, if in 2003, 890 sources were cited for nanoparticles, then in 2023, more than 33 thousand articles on nanotechnology were published.

Of all known elements from the point of view of medical applications, the greatest attention has been paid to elements with variable valence, in particular the lanthanide group. Of this group, the largest number of studies has been devoted to cerium oxide nanoparticles, with 1362 publications in the last 5 years according to the PubMed database, including systematic reviews. Encouraging results indicating antimicrobial, regenerative, and antioxidant effects have been obtained, which makes nanoceria promising for drug development and applications in veterinary medicine and medicine [14–17]. However, the biomedical application of nanoceria in the form of final global products, unlike gadolinium, is still a prospect. Lanthanoid “gadolinium nanoparticles” showed at the same query a reference to only 615 publications for the last 5 years, and the absolute majority of works simply illustrated the high efficiency of gadolinium-based drugs in imaging (CT/MRI) examinations. According to Pubmed data, only 67 studies have been devoted to gadolinium oxide nanoparticles in the last 5 years, and only a few of them are not related to contrasting, which determines the novelty of this field of knowledge. At the same time, taking into account that gadolinium is in the same lanthanide group as cerium, we can expect similar useful biological effects to nanoceria, which are also useful for regenerative medicine.

Gadolinium is a rare earth metal belonging to the lanthanide group (order number 64) with an atomic weight of 157.25 g/mol, has 2 allotropic modifications: - α-gadolinium with a hexagonal tightly packed crystal lattice with a = 3.6336 Å and c = 5.7810 Å at room temperature and β-gadolinium with a cubic volume-centered crystal lattice with a = 4.06 Å at 1265 °C (2309 °F). In nature, the element occurs as a mixture of six stable isotopes. Odd-numbered isotopes have extremely high nuclear absorption cross sections, which explains its bright luminescence in radiological studies, and for gadolinium-157 it reaches 259,000 barns. As a result, the natural mixture of gadolinium isotopes also

 doi:10.20944/preprints202411.1441.v1

has a very high nuclear absorption cross section of about 49,000 barns. For example, cerium has a nuclear absorption cross section 50,000 times smaller.

Gadolinium and its derivatives have been long and widely used as burn-up absorbers in the cores of nuclear reactors, in metallurgy to create alloys with special properties, as luminophores in medical visualization, as a source of gamma radiation in electronic and optical devices. In medical (therapeutic) applications all is much poorer. Nanoparticles containing gadolinium are used to deliver nanoparticles containing gadolinium to the primary tumor focus or its metastases for tumor control, delivery of antitumor drugs and radiotherapeutic sessions of neutron-capture therapy [17–24] or phototherapy based on the same very high nuclear absorption cross section [25,26].

Activated controlled nanoparticles for X-ray irradiation with the inclusion of gadolinium have a double advantage: they imitate the effect of magnetic resonance imaging (MRI) contrast agent used in clinical practice and enhance the radiotherapeutic activity of conventional X-ray radiation [27]. This therapeutic effect is explained, on the one hand, by paramagnetic properties of gadolinium and, on the other hand, by the formation of high density of secondary radiation as a result of interaction between ionizing radiation and atoms with high atomic number, which leads to an increase in radiation dose in tumors where nanoparticles accumulate. The first experience obtained in the treatment of breast cancer in patients with locally advanced cervical cancer and hepatocellular carcinoma is encouraging [28–31].

In addition to tumor diseases, gadolinium oxide nanoparticles have proven themselves in the diagnosis of ischemic and reperfusion myocardial lesions [32,33], in neurology [34,35], orthopedics [36], and hepatology [37]. The fluorescence effect of gadolinium nanoparticles under high-energy radiation has also been proposed for work with cell cultures as intracellular markers that allow observing the fate of each specific cell, which are well identified by MRI and fluorescence microscopy [38,39].

We had the goal of evaluating the potential biomedical applications of gadolinium oxide nanoparticles synthesized under industrial conditions. We believe that Gd_2O_3 nanoparticles hold great promise in the field of regeneration, including tissue engineering. In contrast to nanoceria, gadolinium oxide nanoparticles included in implants will be well visualized, which will make it possible to non-invasively study the evolution of the nanomaterial, which at the same time exhibits beneficial antioxidant properties. Confirmation of anti-apoptotic and antioxidant effects by Gd_2O_3 nanoparticles, which will be useful for accelerating wound healing, is reported in several studies [40–44]. The antioxidant effect of gadolinium nanoparticles was so obvious that there were even attempts to explain their success in the treatment of malignant tumors [45]. Complexes with nanogadolinium may also be useful in antimicrobial applications, which is especially relevant in view of the problem of antibiotic resistance and the wide spread of dangerous hospital infections [46–52]. In addition, the combinatorics of composition and methods for synthesizing of combinatorial compounds containing gadolinium oxide nanoparticles to improve biochemical and biological effects to accelerate wound healing, which are being conducted by many researchers and the results obtained by them, add more and more optimism to this research [53–57].

All of the above strengthened our intention to start an systematic study as a member of a multidisciplinary research group including specialists in chemistry, physics, biology and medicine, and to evaluate the possibilities of using nanogadolinium in other biomedical applications, including related to regenerative medicine.

The aim of the study is to synthesize nanosized gadolinium oxide powder, to evaluate its physicochemical characteristics, to investigate its pro- and antioxidant properties, and to study its effect on cytotoxicity, metabolism, proliferative and migratory activity of different cell lines involved in regeneration (multipotent stromal cells, fibroblasts, keratinocytes).

 doi:10.20944/preprints202411.1441.v1

2. Materials and Methods

2.1. Synthesis of Gadolinium Oxide Nanoparticles

Nanosized gadolinium oxide was obtained in the production conditions of the research and production complex of LLC "LANHIT" by a typical process by thermal decomposition of gadolinium carbonate precipitated from nitrate solution. The processes are described by equations 1-3:

$$Gd_2O_3 + 6HNO_3 \rightarrow 2Gd(NO_3)_3 + 3H_2O \quad (1)$$

$$2Gd(NO_3)_3 + 3(NH_4)_2CO_3 \rightarrow Gd_2(CO_3)_3\downarrow + 6NH_4NO_3 \quad (2)$$

$$Gd_2(CO_3)_3 \rightarrow Gd_2O_3 + 3CO_2\uparrow \quad (3)$$

As initial reagents we used gadolinium oxide Gd_2O_3 with 99.99% purity in terms of metal impurities (metalsbasis) (LANHIT, Moscow, Russia), extra pure nitric acid, chemically pure ammonium carbonate $(NH_4)_2CO_3$ and ammonium nitrate NH_4NO_3. The precipitation was performed from gadolinium nitrate solution with a concentration of 50 g/L gadolinium oxide. A solution of ammonium carbonate $(NH_4)_2CO_3$ with a concentration of 200 g/L was used as a precipitant. In the reaction vessel with volume of 3 L 1 was poured 1 L of freshly prepared ammonium nitrate solution (as a crystallization regulator) with concentration of 4 mol/L, then from one separating funnel was added dropwise 1 L of gadolinium nitrate solution with concentration of 50 g/L, and from another - 500 ml of ammonium carbonate solution with concentration 200 g/L. The solutions of gadolinium nitrate and precipitant were delivered equally and simultaneously into the reaction vessel under continuous stirring with a Hei-TORQUE stirrer (Heidolph Instruments, Schwabach, Germany) at 300-350 rpm for 10 minutes.

After complete delivery of reagents, the obtained gadolinium carbonate was filtered on a Buechner funnel and washed with distilled water on a filter. The temperature of the wash water was 30-40°C and the volume was 2 liters. Then the precipitate was dried in air at 25-35°C for 2-3 days to obtain a bulk product.

Decomposition of carbonate was carried out in a quartz crucible placed in a muffle furnace at 650°C for 3 hours. After cooling, the obtained gadolinium oxide was sieved through a polyamide fiber mesh with a mesh size of 0.1 mm.

Powders and aqueous suspensions (solvent - water for injection) of Gd_2O_3 NPs in a wide range of concentrations - from 3.6 g/L (10^{-2}M) to 0.0005 g/L (10^{-6}M) taking into account the molecular weight of Gd_2O_3 362.5 g/mol - were prepared for physicochemical and biological methods of investigation.

For biological studies, each concentration of nanogadolinium was prepared in an individual tube. For this purpose, the powder of Gd_2O_3 NPs with sterile water for injection was stirred on a magnetic stirrer for 30 min, after which it was dispersed in an ultrasonic bath for 20 min and then it was centrifuged at 4,000 rpm for 10 min to select the smallest fraction of nanoparticles. Next, the concentration in the final suspension was determined by thermogravimetry, after which 4 final concentrations of Gd_2O_3 NPs were created for cell culture studies: 10^{-2}M, 10^{-3}M, 10^{-4}M, 10^{-5}M.

2.2. Physicochemical Methods of Research

The synthesized powder of Gd_2O_3 NPs was analyzed by mass spectrometry, transmission electron microscopy (TEM), X-Ray Diffraction (XRD), Raman spectroscopy, scanning electron microscopy (SEM) with energy dispersive X-ray analyzer (EDX). Liquid forms of nanogadolinium (suspensions of different concentrations) were investigated for redox activity using optical spectroscopy (OS) method in the photochemical degradation process of methylene blue dye upon irradiation with an optical source.

The size of Gd_2O_3 particles was determined by transmission electron microscopy (TEM) on a JEM2100 device at an accelerating voltage of 200 kV (JEOL, Akishima, Japan). Overview images were obtained at magnifications (x10,000 - 20,000). For more detailed study of the structure and observation of traces of atomic planes we used direct magnification x400,000 - up to 1.5 million times,

 doi:10.20944/preprints202411.1441.v1

the maximum approximate ruler on microphotographs - 10 nm. Selector apertures were used to select areas and obtain diffraction patterns.

Image J and Statiatica program were used to estimate the average size of nanoparticles. The diameters of 200 nanograins in different grid regions were measured, after which the variance was divided into equal size intervals, finally a frequency histogram was constructed and the average size of nanoparticles was determined.

The X-ray diffractogram (XRD) of the Gd_2O_3 NPs powder sample was measured at room temperature using a GBC EMMA X-ray diffractometer (Scientific Equipment, Victoria, AU) at wavelength λ = 1.5401 Å of the CuKα line in θ-2θ geometry with 0.02° step. The obtained data were processed using the Rietveld method with the PowderCell program [58]. The theoretical diffractogram was calculated from the structural parameters of the Gd_2O_3 lattice determined in [59] from synchrotron radiation diffraction experiments.

The vibrational Raman spectroscopy was performed on a confocal Omega Scope TM Raman spectrometer (AIST-NT Inc., Edison, NJ, USA). Excitation was performed with a laser with a wavelength of 532 nm, with a power of 30 mW in the region of 150 - 1000 cm^{-1}. A diffraction grating with a density of 1800 mm^{-1}, providing a spectral resolution in the measured region of 0.8 cm^{-1}, was used to obtain the spectrum of excited radiation.

The impurity composition of the initial and obtained oxides was analyzed by Spark Source Mass Spectrometry with dual focus JMS-01-BM2 (JEOL, Akishima, Japan). The high-resolution mass spectra were photographed on Ilfrod-Q plates. A Joyce Loebl (United Kingdom) MDM6 microdensitometer and a NOVA 4 (USA) on-line mini-computer were used for the mass spectrum lines identification. Quantification was calculated using MS&GCLab software. Noble gases and transuranic elements have not been tabulated because their concentrations were lower than detection limits (<0.01 ppm). The impurity content was presented as parts per million relative to the metal matrix (1 ppm = 0.0001%). The mass of powder sent for the study was 25g.

SEM. Surface morphology and structure features, as well as the distribution and quantitative composition of chemical elements in the studied samples were investigated using a scanning electron microscope JSM-6610LV (JEOL Ltd., Akishima, Japan) in high-vacuum mode. The spatial resolution of the microscope in high vacuum mode was 3 nm. The accelerating voltage was 20 kV. For elemental analysis, the studies were carried out using a characteristic X-ray detector (XRMS/EDS - X-ray spectral microanalysis), which allows studying on the surface of samples microspectral distributions of chemical elements in the range from Be (Beryllium) to Pu (Plutonium). The active area of the silicon window of the X-Max Silicon Drift Detector, Oxford Instrments, Great Britain was 20 mm^2. The stability of the detector resolution and the stability of the peak positions in the spectrum were not less than ±1eV.

The antioxidant and prooxidant properties of Gd_2O_3 NPs in a wide range of concentrations were investigated using an HR-2000 optical spectrometer (Ocean OpticsInc, Dunedin, FL, USA) during photooxidative degradation reaction of methylene blue dye (Himedia Laboratories Pvt. Ltd, Maharashtra, India), which was both a photosensitizer (with absorption maximum at the wavelength of 662 nm) and an indicator of the process. At irradiation of methylene blue by a light source with a wavelength of 660 nm due to strong absorption of optical photons by the dye, there was photogeneration of electron-hole pairs initiating a cascade of oxidation-reduction reactions in solution with the formation of active radicals. In this case, degradation of methylene blue and highlighting of the solution based on it occurred due to the formation of highly active oxygen radicals, in particular short-lived hydroxyl radicals, which attacked methylene blue molecules and destroyed its coloring centers.

Irradiation of methylene blue solutions was carried out using a red light-emitting diode source in a narrow spectral range with a wavelength of 660±5 nm. The irradiation dose was 80 J/cm2. Kinetic dependences of the photodegradation process in all cases corresponded to the pseudo-first order reaction. The activity of photodegradation processes was characterized by the reaction rate constant according to formula (4):

 doi:10.20944/preprints202411.1441.v1

$$k = -\ln(\frac{C}{C_0})/t \quad (4)$$

When Gd_2O_3 NPs were added, their antioxidant or pro-oxidant properties were manifested, leading to either a slowing down or acceleration of the reaction rate of dye degradation, respectively.

2.3. Biomedical Methods of Research

The study was performed using different cell lines involved in wound healing (on cell cultures of human keratinocytes, human fibroblasts, and human mesenchymal stem cells) to determine the regenerative potential of Gd_2O_3 NPs.

First, Gd_2O_3 NPs were tested to evaluate the effects of different concentrations (10^{-2} to 10^{-6}M) on the metabolic and proliferative activities of human fibroblasts (MTT test, direct cell counting after 72 h of co-culture). Visualization of cells under light microscopy showed unaffected agglomeration of nanoparticles at high concentration and difficulty in performing cell counting and their focusing (at a concentration of 10^{-2}M). In this regard, in a second step, the same series of experiments (MTT test, direct cell counting with visualization and cell viability assessment) were performed on human keratinocyte culture after 72 hours of co-culture with nanoparticles at concentrations of 10^{-3}M, 10^{-4}M, 10^{-5}M and 10^{-6}M.

Based on the obtained data from the above series of experiments on fibroblasts and keratinocytes, the best (promising) concentration of Gd_2O_3 NPs (10^{-4}M) was selected and a test was performed to evaluate migration activity on a culture of human mesenchymal stem cells on a model wound.

2.3.1. Methods for Evaluating the Effect of Different Concentrations of Aqueous Suspensions of Gd2O3 NPs, on Cytotoxicity/Biocompatibility, Metabolic, Proliferative Activity of Human Fibroblasts and Keratinocytes

2.3.1.1. Cell Lines of Fibroblasts and Keratinocytes and Their Cultivation

Human fibroblast cell line BJ TERT, source - American Type Culture Collection ATCC (Manassas, Virginia, USA). The cells belong to the hTERT-immortalized type obtained by transfection of the BJ fibroblast cell line with a plasmid expressing telomerase reverse transcriptase (hTERT).

Human keratinocytes from the HaCaT cell line, which are spontaneously immortalized non-cancerous human keratinocytes, are capable of unrestricted division while exhibiting normal differentiation [60,61]. Cell source: adult human skin. Line origin: FSBI N.N. Blokhin National Medical Research Center for Oncology of the Ministry of Health of the Russian Federation (Moscow, Russia).

Human fibroblasts of the BJ TERT line were cultured in commercially treated Petri dishes d 100 mm (SPL Life Sciences, Korea) in DMEM medium containing at least 4.5 g/L glucose (PanEco, Russia) supplemented with 10% fetal calf serum (Global Kang Biotechnology, China), 146 mg glutamine (PanEco, Russia), and 1% penicillin, 1% streptomycin (PanEco, Russia). Cells were incubated at 5% CO_2 concentration in ambient air at 37ºC and controlled humidity under standard CO_2-incubator conditions (Binder, Germany). When the fibroblasts reached 100% confluency, the next passage of cell culture was performed; the medium was changed after three days from the moment of passage. Cultivation of human fibroblasts of BJ TERT line was performed according to the standard protocol.

Then, according to the design of the experiment, human fibroblasts were seeded into 24-well plates (SPL Life Sciences, Korea) at a cell concentration in suspension of $5.0x10^4$/ml, counting was performed in a standardized method using Countess II Automated Cell Counter (ThermoScientific, Waltham, MA, USA). Cells were placed into wells in a volume of 900 µl. After 24 hours of cultivation under standard CO_2 incubator conditions, 100µL per well were added to the fibroblasts at the appropriate concentrations, and the coincubation was continued under the standard conditions described above for the next 72 hours.

Cells were cultured in culture Petri dishes (SPL LifeSciences, Korea) in DMEM medium with high glucose content (at least 4.5 g/L) (PanEco, Russia), supplemented with 10% fetal calf serum (Global Kang Biotechnology, China), 146 mg glutamine (PanEco, Russia) and 1% penicillin, 1%

 doi:10.20944/preprints202411.1441.v1

streptomycin (PanEco, Russia). Cell cultures were incubated in a CO2 incubator (Binder, Germany) under standard controlled conditions (5%CO2, 37ºC) and controlled humidity. Passage of HaCaT keratinocytes was performed every 3 days according to the standard protocol. For the experiment, cells were seeded in 24-well plates (SPL LifeSciences, Korea) using DMEM medium according to the standard protocol at a concentration of cells in suspension of 7.0 x104/ml. After 24 hours, the test substances (nanogadolinium of different concentrations – 10ob%) were added and co-incubation was continued for the next 72 hours. The initial solvent, which was sterile water for injections, was added as a control.

2.3.1.2. MTT-Test

To assess the metabolic activity of cells, a colorimetric MTT-test was performed, during which yellow tetrazole, was reduced in living cells into purple formazan. The amount of formazan formed as a result of this reaction was proportional to the number of viable cells in the well.

After 72 hours of co-incubation with nanosubstances, the culture medium was removed from the wells and 3% MTT reagent (PanEco, Russia) was added. To realize the intracellular reaction, the plate with the reagent was placed at 37ºC for 30 minutes. The MTT working solution was then removed and dimethyl sulfoxide (DMSO, neoFroxx, Germany) was added as a solubilizing agent. The plate was incubated at room temperature on an oscillating shaker (Elmi-S4, Latvia) for 5 minutes, then the dissolved contents were transferred in a volume of 100 µl into a 96-well plate to measure the optical density at 540 nm spectrophotometrically (Multiscan Labsystems, Finland). The final result was expressed in relative optical density (OD) units.

Each sample was tested in 12 wells. Injection water was used as a control, which was added in a similar amount (100 µl to a total volume of 1000 µl) also in 12 wells.

2.3.1.3. Determination of Proliferative Activity and Dead/Living Cells Ratio with Trypan Blue Staining

Cell counting was performed automatically using Countess II Automated Cell Counter (Thermo Scientific, Waltham, MA, USA), which reflected the quantitative composition of the cell suspension and made it possible to identify viable cells in the population. This method consisted in visualizing and recognizing cells after they were stained with special dyes that penetrated the cytoplasm when the cell wall was damaged. At the end of the incubation period, the medium was removed from the plate and the cell wells were washed with phosphate-salt buffer. Next, cells were detached by adding trypsin-Versen solution in a 1:3 ratio (PanEco, Moscow, Russia) for 1 minute at 37ºC. Then 10 µl of trypan blue dye (PanEco, Moscow, Russia) was added to the cell suspension and mixed by pipetting. The stained cell suspension was added to the slide for automatic counting and fixation of cell viability. As a result, the total concentration of cells in 1 ml and the percentage of live and dead cells were counted.

Each sample was examined in 7 wells. Injection water was used as a control, which was added in a similar amount (100 µl to a total volume of 1000 µl) also in 7 wells.

2.3.2. Study of Migration Activity and Rate of Healing of a Model Wound In Vitro on Human Mesenchymal Stromal Cell Culture

2.3.2.1. Culture of Human Adipose–Derived Mesenchymal Stromal Cells

Human mesenchymal stromal cells (MSC) lines were used in this study. MSCs were previously generated in our laboratory using the method [62]. Cells at passage 3 and 4 were used for experiments.

MSCs were cultured in a humidified atmosphere containing 5% CO2 at 37 °C on standard plastic dishes for cell culture (Corning Costar, Corning, NY, USA) in Dulbecco's Modified Eagle Medium/Nutrient Mixture F-12 (DMEM/F12; Thermo Fisher Scientific, Waltham, MA, USA) supplemented with 100 U/mL penicillin and streptomycin, 2 mM L-glutamine (Paneco, Moscow, Russia), and 10% fetal bovine serum (One Shot FBS; Gibco, Thermo Fisher Scientific, Waltham, MA, USA) until ~70-80% confluence. The medium was changed every 3-4 d. Then MSCs were passaged

 doi:10.20944/preprints202411.1441.v1

with trypsin/EDTA solution (Paneco, Moscow, Russia). The identity of expanded MSCs was confirmed by the minimal criteria proposed by The International Society for Cellular Therapy [63].

MSCs from passage 3 attached to the plastic surface were positive for CD73, CD90, and CD105 expression and negative for CD34, CD45, and CD14 expression. These cells were able to differentiate into adipogenic, osteogenic, and chondrogenic lineages under special conditions as described in [62].

2.3.2.2. Methodology for Assessment of Migration Activity and Rate of In-Vitro Model Wound Healing on Human MSCs

The migration rate of MSCs was assessed upon the addition of Gd2O3 NPs at concentrations of 10^{-4}M. The cells in the medium alone were used as acontrol. The scratch size was initially set to be 100%, and wideness was measured at different time points - immediately after adding NPs (point 0), after 24 hours, 48 hours and 72 hours.

MSCs were grown under the same conditions as those described in the previous section. The cell layer was then scratched across the diameter of 35 mm Petri dishes using 200 μL pipette tips (Greiner Bio-One, Kremsmunster, Austria). The culture medium was then immediately removed (along with any dislodged cells) and replaced with 1.5 mL of DMEM/F-12 containing 10% FBS, with the addition of 10^{-4} M Gd_2O_3. Images from the same viewpoint were obtained under microscopy at the baseline (0 h) and every 24 h after wounding for determination of the extent of wound closure. ImageJ 1.49v (National Institutes of Health, Bethesda, MD, USA) was used to measure the void area, and the extent of the wound closure was evaluated (width (%) = void area /baseline area) in each group.

At each control point (0, 24 h, 48 h, 72 h), four measurements were performed by two independent people using the same method, thus obtaining 12 quantitative variables for each group at each time point.

2.4. Statistical Data Processing

Statistical processing of the results of the study on cell lines was performed using the statistical program SPSS 25.0 (IBM Corp., Armonk, NY, USA).

First of all, the normality of the distributions of MTT-test and cell count indices for each of the samples was assessed by the Kolmogorov-Smirnov and Shapiro-Wilk criteria. The normality test proved the obedience to the law of normal distribution ($p>0.05$).

Descriptive statistics of continuous quantitative measures were presented as Mean, Std. Deviation, Std. Error, 95% Confidence Interval for Mean (95CI), Minimum, Maximum. The t-test was used to compare only two groups. One-factor ANOVA analysis of variance was performed for comparative analysis of the different subgroups. A posteriori multiple comparisons were performed using the Dunnett test (for comparison with the control). Differences were considered statistically significant when *p*-value <0.05.

3. Results

3.1. Results of Evaluation of Physicochemical Characteristics of Gadolinium Oxide Nanoparticle Powder

3.1.1. Transmission Electron Microscopy

The study of $Gd_2O_3$by transmission electron microscopy (Figure 1) showed that the shape of the particles was close to cubic. The size of the nanoparticles ranged from 2 nm to 43 nm, with the maximum of the distribution corresponding to 15-25 nm. Gd_2O_3 particles with a diameter ≤10 nm were 18%. The average size of the nanoparticles was 23±9 nm.

 doi:10.20944/preprints202411.1441.v1

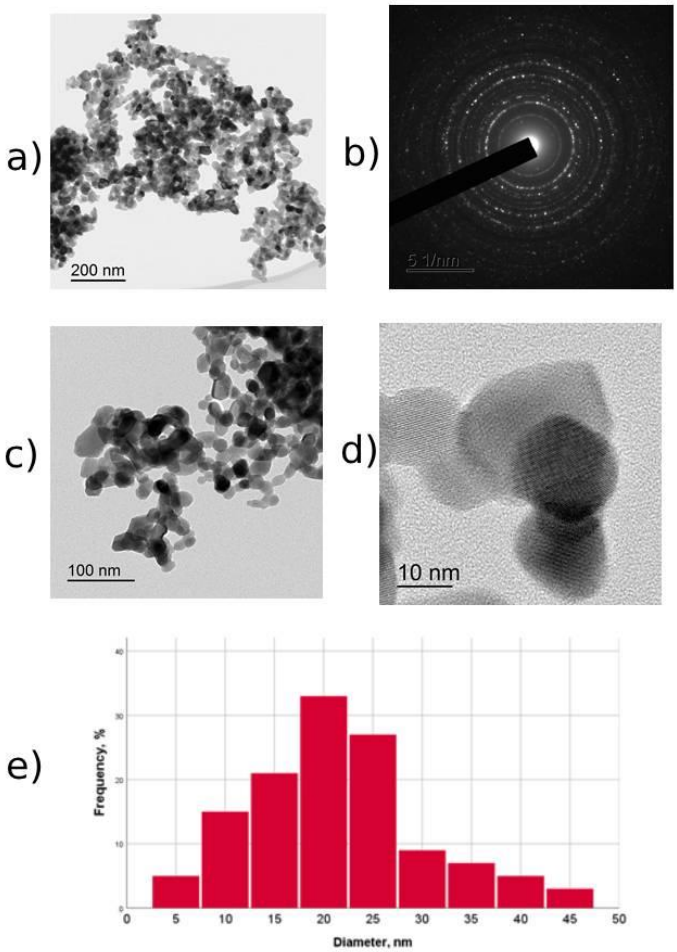

Figure 1. TEM images of powder Gd_2O_3 NPs, obtained on microscope JEM-2100 at accelerating voltage 200 kV: **(a)** - overview image of agglomerate and **(b)** its electronogram; **(c, d)** - enlarged image before visualization of separate nanoparticles with scale bar 100 nm - 10 nm; **(e)** - grain size distribution of Gd_2O_3 NPs.

3.1.2. X-Ray Diffraction

X-ray phase analysis (XRD) showed (Figure 2) that almost all diffraction peaks, both in position and intensity, correspond to the cubic structure (C-form) of Gd_2O_3 ($Ia\bar{3}$, p.g. 206) with the lattice parameter a = 10.79(9) Å, which is very close to the values obtained earlier for the nanoscale powder Gd_2O_3: 10.8175 Å [59], 10.813 Å [64]. However, a small number of weak diffractions were present in the diffractogram, which could indicate the presence of defects in the crystal structure and the manifestation of forbidden diffractions.

The coherent X-ray scattering length D, was determined by the Debye-Scherrer formula: $D = K\lambda/(\beta\cos\theta)$, where θ is the Bragg angle, λ is the X-ray wavelength, β is the half-width (width at half-height) of the diffraction peak, K is a coefficient depending on the particle shape, which can vary from 0.6 to 2.1. If the particle shape is close to cubic, K depends on the moduli of the indices of the plane (*hkl*) from which the diffraction occurred: $K = 6h^3/[(h^2+k^2+l^2)^{1/2}(6h^2-2(k+l)h+kl]$ [65]. The value of crystallite size in the studied sample of Gd_2O_3 determined by diffractions with the highest intensity was 23±3 nm.

 doi:10.20944/preprints202411.1441.v1

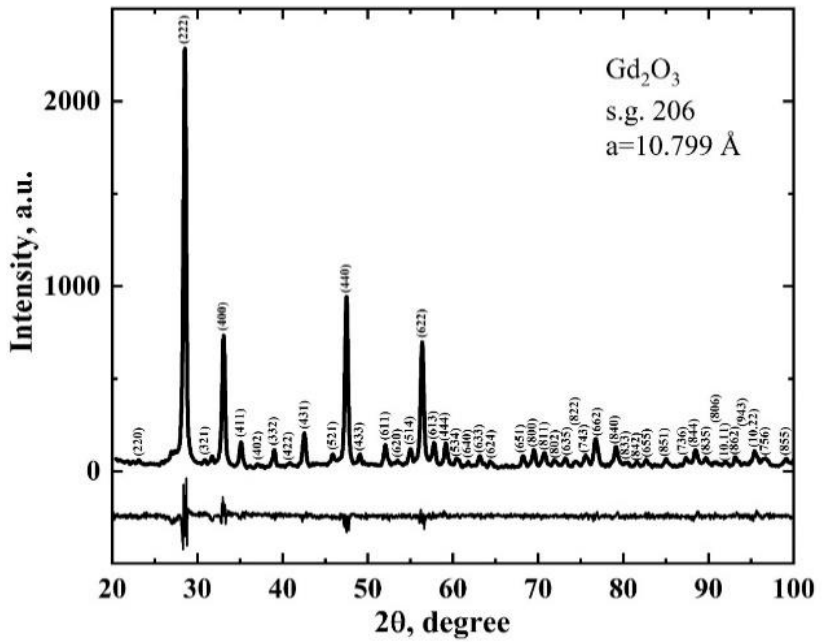

Figure 2. Diffractogram of a sample of Gd_2O_3 powder. The upper graph represents the experimental curve with indexing of peaks by the corresponding planes from which the diffraction occurred. The lower graph represents the difference between the experimental and theoretical diffractograms.

3.1.3. Raman Spectroscopy

Raman spectra of Gd_2O_3 powder are shown in Figure 3. According to the group-theoretic analysis $Ia\bar{3}$, there are 22 allowed Raman vibrations for the cubic structure - these are modes 4Ag, $4E_g$ and 14 F_g [66]. Due to the large difference in the weight of Gd and O ions, the Raman spectrum of Gd_2O_3 is divided into three regions: (1) at frequencies less than 250 cm^{-1}, the vibrations of heavy gadolinium ions predominate; (2) in the range from 250 cm^{-1} to 500 cm^{-1}, the vibrations across the bends (bendingvibrations) of Gd-O are the main ones; (3) in the region 550 - 1000 cm^{-1}, the vibrations along the bends (stretchingvibrations) of Gd-O may be observed. Since the allowed Raman modes are quite numerous, oscillations corresponding to the combination of phonon modes (with total or difference frequencies) should be observed in all the above-mentioned regions of the spectrum. The region above 1000 cm^{-1} was not investigated by us because it does not characterize the lattice vibrations, but it can be used in the analysis of the luminescence response from impurity centers [67]. The measured Raman spectrum (Figure 2) was consistent with previously observed Raman spectra for single crystals, films and nanoparticles of Gd_2O_3 [68,69]. The obtained spectrum contained peaks in all three regions described above, and their position was in good agreement with the position of Raman active modes (the strongest of which are marked in Figure 3) and with the position of modes caused by the main vibrations of atoms in the crystal lattice (Gd-Gd and Gd-O) or their combinations, which spoke about the structural quality of Gd_2O_3 nanocrystals.

According to the parameters of the strongest Raman mode, we can estimate the size of Gd_2O_3 nanoparticles using the correlation from [70]: FWHM (cm^{-1}) = 10+124.7/D (nm), where FWHM is the half-width of the main Raman mode and D is the crystallite size. For the mode 356 cm^{-1}, FWHM = 15.9 cm^{-1} and, respectively, the average size of the Gd_2O_3D ≈21 nm, which was almost in agreement with the values determined from TEM experiments and XRD analysis.

As shown by detailed analysis of the Raman spectrum, in Gd_2O_3 the spectral region ω> 1000 cm^{-1} did not characterize the lattice vibrations, but was used in the analysis of the luminescence response from impurity centers [67], since the photoluminescence efficiency of rare-earth metal impurities in their oxides can be quite high [71–74] due to the effect of energy transfer from the cation to the impurity ion. The inset to Figure 3 shows a part of the Raman spectrum containing photoluminescent peaks. They are well identified with the energy transitions involving impurity ions Eu^{3+}: the transitions $^5D_0$-$^7F_1$ and $^5D_0$-$^7F_2$ are formed due to magnetic and electric dipole interactions, respectively, and the transitions $^5D_0$-$^7F_0$ for ideal

 doi:10.20944/preprints202411.1441.v1

crystals are forbidden by the selection rules, but in real crystals and, even more so, nanoparticles due to distortions of the crystal field these transitions can be observed [74].

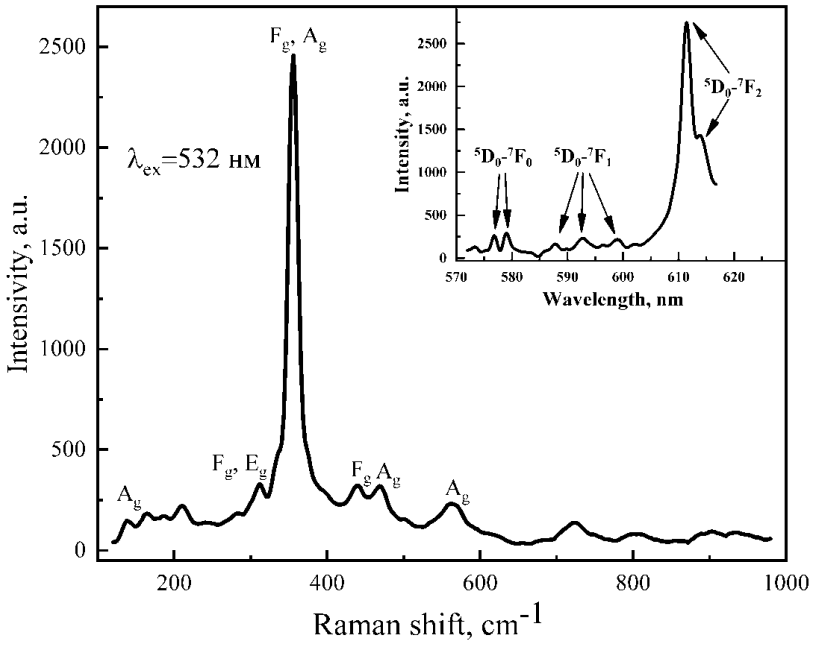

Figure 3. Raman spectrum of Gd_2O_3 powder with identification of the main Raman active modes. Inset photoluminescence spectrum of the sample near the wavelength of excitation radiation with marked energy transitions due to the presence of Eu^{3+} ions in the crystal lattice of Gd_2O_3.

3.1.4. Scanning Electron Microscopy and Energy Dispersive Analysis of Secondary (Characteristic) X-Rays

SEM images (Figure 4) show that the powder consisted mainly of agglomerates. The size of the constituent Gd_2O_3 nanoparticles could be evaluated only at high magnifications; on average, the size of the nanoparticles was not more than 30 nm. The average size of agglomerates was 30 μm, the maximum size was 60 μm, and the minimum size was 10 nm.

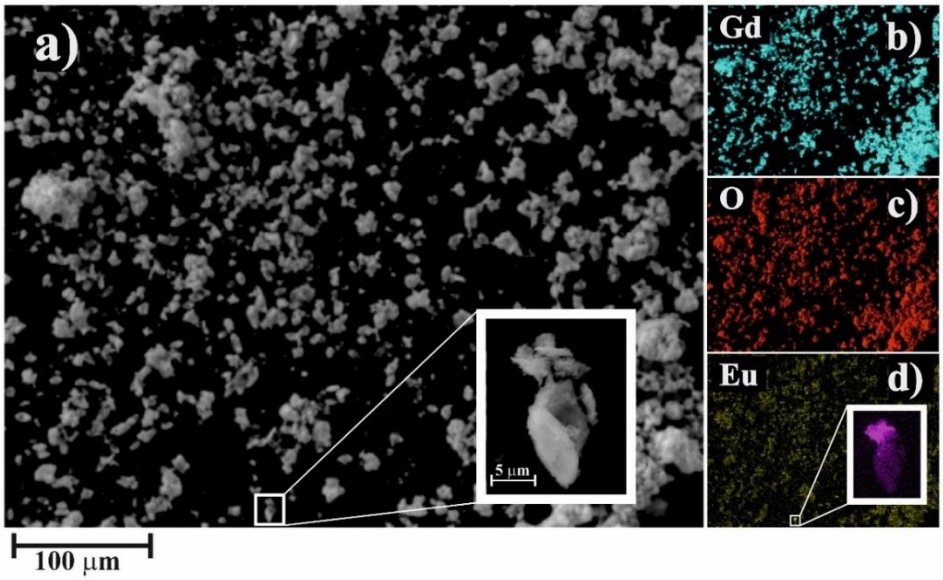

Figure 4. Images of Gd_2O_3 powder particles obtained by scanning electron microscopy (a) and elemental distribution maps: Gd (b), O (c) and Eu (d). The insets show the image of the agglomerate with increased Eu content.

 doi:10.20944/preprints202411.1441.v1

Energy dispersive analysis of secondary X-rays was used to determine the elemental composition. The composition of the powder was within the measurement error (0.2% at.) equal to the stoichiometric composition (Figure 4b, c) when scanning on small scales (multiplicity 500 - 100), and the presence of impurity was detected only with multiple scans of the investigated area. In the overwhelming part of agglomerates its concentration was much less than 0.2 % at. And could not be accurately estimated by the used methodology. However, when plotting the europium distribution map, single agglomerates containing europium in increased amounts were clearly visible (Figure 4a, 4d insets). On average for such particles, the europium concentration reached 4.5 % at. While maintaining the stoichiometry of the initial compound.

3.1.5. Mass Spectrometry

The study of purity of synthesized gadolinium oxide nanopowder by mass spectrometry data showed that the product contained the following main impurities: rare-earth metals – Ho (20 ppm), La (6 ppm), Eu and Tb (3 ppm), Tm (2 ppm), Sm (1 ppm), others – up to 1 ppm, all rare-earth metals – less than 15 ppm (Table 1). The final purity of the product Gd_2O_3 was 99.9%.

Table 1. Mass spectroscopy results, in parts per million (ppm).

Element	Gd_2O_3	Element	Gd_2O_3
Na	< 0.5	La	6
Mg	1	Ce	<0.1
Al	5	Pr	0.6
Si	<10	Nd	<0.1
K	0.6	Sm	1
Ca	0.8	Eu	5
Ti	<0.01	Tb	3
V	<0.01	Dy	< 0.1
Cr	<0.01	Ho	20
Mn	1	Er	< 0.1
Fe	1	Tm	2
Co	<0.02	Yb	< 0.1
Ni	<0.02	Pb	< 0.2
Cu	1	Bi	< 0.2
Zn	2	Th	< 0.2
Y	0.6	U	< 0.1

3.2. Result of Evaluation of The Redox Activity of Gd_2O_3 Nps at Different Concentrations

Figure 5 shows the results of the redox activity of Gd2O3NPs in the photooxidative degradation process of methylene blue dye under red light irradiation. The change in the reaction rate was determined and calculated by the formula $\Delta k_{Gd_2O_3} = k_{MB+Gd_2O_3} - k_{MB}$. The minus sign on the auxiliary Y axis of the figure indicates that the degradation reaction of methylene blue is slowed down in the presence of Gd_2O_3 nanoparticles with a concentration ≤ 10^{-3}M. The figure shows that Gd_2O_3 NPs generally had a weakly pronounced antioxidant activity, which depended on the concentration of particles in solution. Thus, the highest antioxidant activity was observed for particles with a concentration of 10^{-3}M, when the photodegradation rate constant of methylene blue decreased by 5.5% to 9.4·10-3 min^{-1}. When the particle content was reduced to 10^{-5}M, the antioxidant activity decreased to 2.2%, due to the decrease in the amount of active ingredient. Interestingly, as the concentration increased above 10^{-3}M, a decrease in antioxidant activity was also observed, and at a concentration of 10^{-2}M, the activity of Gd_2O_3 NPs became pro-oxidant, accelerating the reaction rate of methylene blue degradation by 15%.

 doi:10.20944/preprints202411.1441.v1

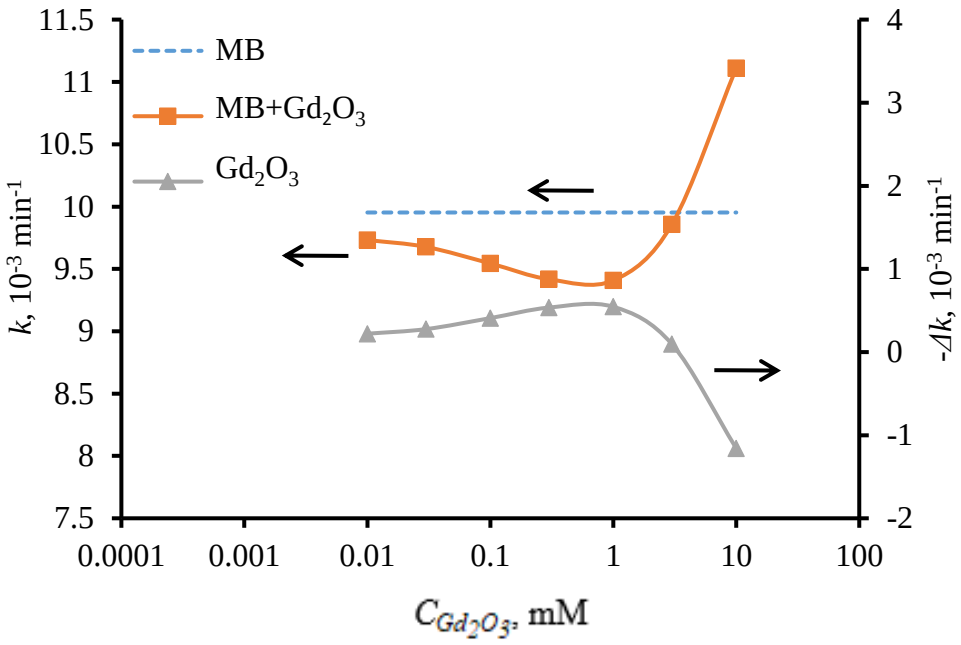

Figure 5. Dependence of the photodegradation rate constant of methylene blue and its variation on the concentration of Gd_2O_3 NPs under red light irradiation. Dashed line (MB)- methylene blue without addition of Gd_2O_3 NPs.

It is noted in [75,76] that lanthanide oxides may exhibit dose-dependent antioxidant activity due to changes in the degree of oxidation of cations on the oxide surface. This may explain the manifestation of weak antioxidant properties of Gd_2O_3 NPs at concentrations of 10^{-3}M and below. However, at high particle concentration of 10^{-2}M, the sign of chemical activity was reversed, the particle activity became pro-oxidant, which was possibly due to a competing process. For Gd_2O_3 NPs, this process can be related to the presence of impurity elements (Ho, Eu, Yb) in the crystal matrix of gadolinium oxide, which generate additional energy levels inside the forbidden band of gadolinium oxide.

3.3. Results of Biological Studies on Cell Lines

3.3.1. Results of Studies of the Effect of Different Concentrations of Aqueous Suspensions of Gd_2O_3 NPs, on Cytotoxicity, Metabolic, Proliferative Activity of Human Fibroblasts

According to the MTT test, we found that Gd_2O_3 NPs sols significantly activated the metabolism of human fibroblasts in a wide range of concentrations (10^{-2} - 10^{-4}M) (Figure 6), without affecting on their proliferation at all concentrations that we studied (Figure 7). Interestingly, the greatest increase in OD was recorded when co-cultured with the highest concentrations of nanogadolinium (the increase in metabolic activity was on average 1.28-fold at 10^{-2}M concentration ($p<0.001$) and 1.27-fold with 10^{-3}M relative to control wells ($p<0.0001$). At the same concentrations, a tendency for better proliferative activity was determined. When the concentration of Gd_2O_3 NPs was reduced to 10^{-4}M and 10^{-5}M, the OD index exceeded the control on average by 1.10 and 1.07 times, respectively, but the proliferative activity at low concentrations was characterized by an unreliable tendency to decrease by 7-10% (Table 2).

 doi:10.20944/preprints202411.1441.v1

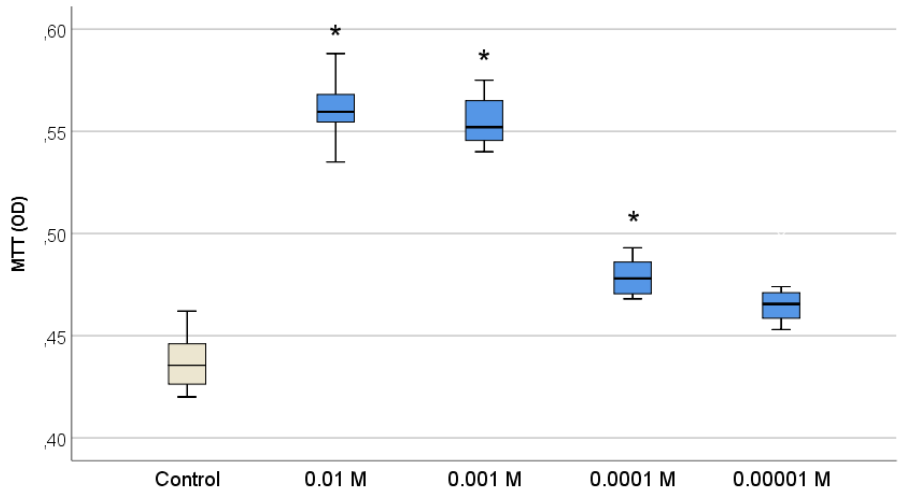

Figure 6. Effect of different concentrations of Gd_2O_3 NPs on metabolic activity of human fibroblasts in MTT test (ANOVA OD:F=184,3; df4, p<0.001; *- difference from Control at p<0.001, Dunnett post hoc tests).

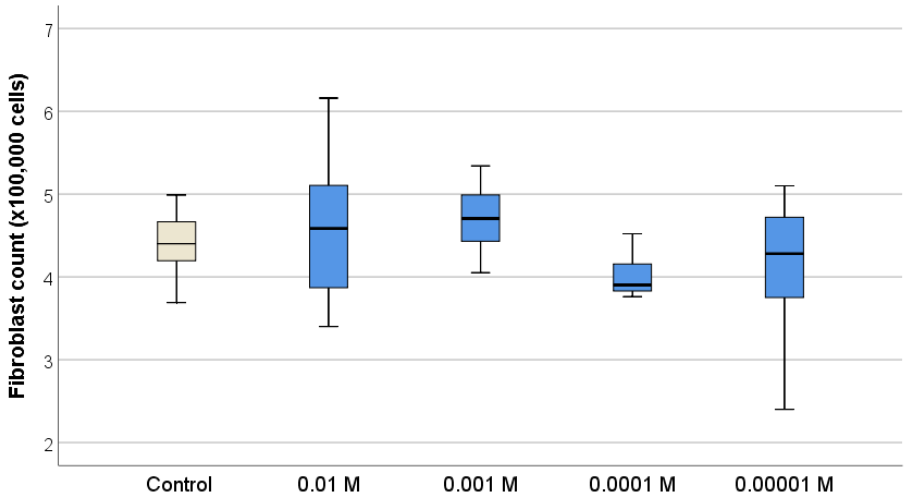

Figure 7. Effect of different concentrations of Gd_2O_3 NPs on proliferative activity of fibroblasts by direct cell counting using an automated cell counter (ANOVA OD:F=1,34; df4, p=0,278).

Analysis of the percentage of dead cells when Gd_2O_3 NPs were co-cultured at different concentrations showed no cytotoxicity. The percentage of dead cells did not exceed 3% and was detected in single (0-1 out of 7, i.e. 0-14%) samples, which indicated in favor of biocompatibility of Gd_2O_3 NPs in a wide range of concentrations (10^{-2} - 10^{-5}M) (Figure 8). Importantly, there was no increase in the number of dead cells or decrease in activity relative to control, even when co-cultured with large agglomerates, which was only detectable at a concentration of 10^{-2}M (Figure 8f). On the contrary, we have to state that even agglomerated nanogadolinium was safe and biosimilar to human fibroblasts.

 doi:10.20944/preprints202411.1441.v1

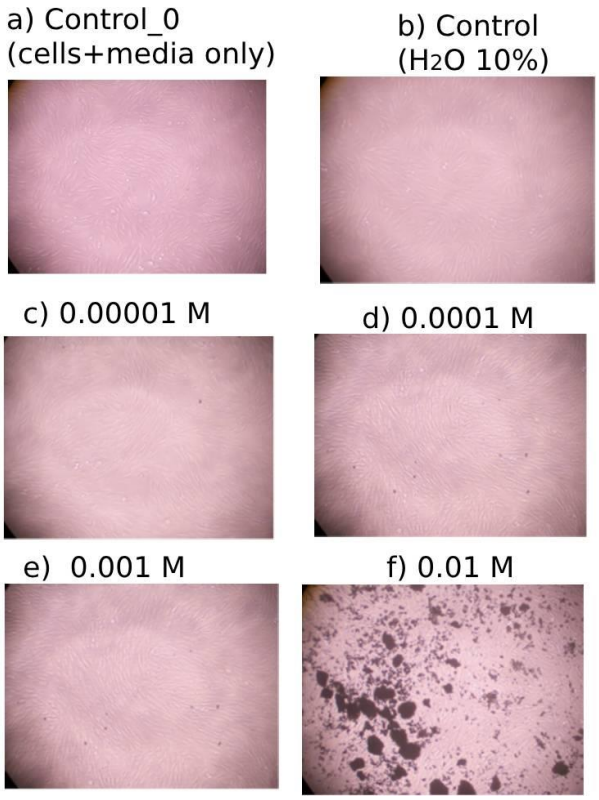

Figure 8. Human fibroblasts after 72-hour incubation with different concentrations of Gd_2O_3 NPs compared to control, magnification ×10.

Table 2. Descriptive statistics of the results of in-vitro studies on human fibroblast culture when co-cultured with gadolinium oxide nanoparticles at different concentrations.

	Mean	Std. Deviation	Std. Error	95% Confidence Interval for Mean		Minimum	Maximum
				Lower	Upper		
MTT, optical density value (OD)							
Control_0	0.432	0.011	0.005	0.425	0.438	0.423	0.453
Control (H_2O)	0.441	0.014	0.006	0.433	0.448	0.420	0.462
Control (average)	0.437	0.013	0.004	0.428	0.445	0.420	0.462
Gd_2O_3 (10^{-2}M)	0.560	0.017	0.005	0.548	0.570	0.524	0.588
Gd_2O_3 (10^{-3}M)	0.556	0.012	0.003	0.548	0.563	0.540	0.575
Gd_2O_3 (10^{-4}M)	0.479	0.009	0.003	0.473	0.485	0.468	0.493
Gd_2O_3 (10^{-5}M)	0.467	0.017	0.005	0.456	0.478	0.435	0.501
Total	0.499	0.051	0.006	0.486	0.512	0.420	0.588
Number of fibroblasts, x100,000 cells							
Control (average)	4.40	0.453	0.171	3.98	4.82	3.69	4.99
Gd_2O_3 (10^{-2}M)	4.59	0.968	0.366	3.69	5.48	3.40	6.16
Gd_2O_3 (10^{-3}M)	4.71	0.452	0.171	4.29	5.12	4.05	5.34
Gd_2O_3 (10^{-4}M)	4.02	0.287	0.108	3.75	4.29	3.76	4.52
Gd_2O_3 (10^{-5}M)	4.10	0.930	0.352	3.24	4.96	2.40	5.10
Total	4.36	0.691	0.117	4.13	4.60	2.40	6.16

Thus, Gd_2O_3 NPs stimulated fibroblast metabolism to the highest degree at concentrations of 10^{-2} - 10^{-3}M (27% enhancement), i.e. it enhanced the production of interstitial substance during

 doi:10.20944/preprints202411.1441.v1

regeneration (collagen, elastin) without affecting the proliferation of human fibroblasts, demonstrating high biocompatibility. The complex analysis of the obtained data allows us to give preference to the concentration of 10^{-3}M as the best dose of nanogadolinium for stimulation of fibroblasts for regenerative purposes.

3.3.2. Results of Studies of the Effect of Different Concentrations of Aqueous Suspensions of Gd_2O_3 NPs, on the Cytotoxicity/Biocompatibility, Metabolic, Proliferative Activity of Human Keratinocytes

It was found that Gd_2O_3 NPs also stimulated keratinocyte cells - analogs of the surface layer of the skin. According to the MTT test Gd_2O_3 NPs at all concentrations (10-3M - 10-5M) contributed to the intensification of human keratinocyte metabolism (Figure 9), tending to slightly increase activation as the concentration decreased (the highest level of OD was recorded at concentrations of 10^{-4} - 10^{-5}M). Analysis of keratinocyte number after 72 hours of cultivation proved the growth of proliferative activity of keratinocytes only at one concentration of Gd_2O_3 NPs (10^{-4}M). The number of cells was on average 1.37 times higher relative to the control ($p<0.01$) (Figure 10; Table 3).

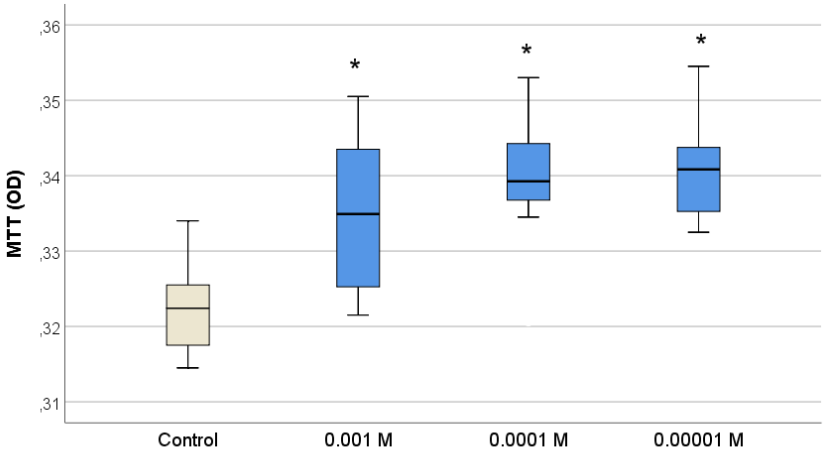

Figure 9. Effect of different concentrations of Gd_2O_3 NPs on metabolic activity of human keratinocytes (BJTERT cells) in MTT test (ANOVA OD:F=5,88; df 3, p=0,004; *- difference from Control at p<0.001, Dunnett post hoc tests).

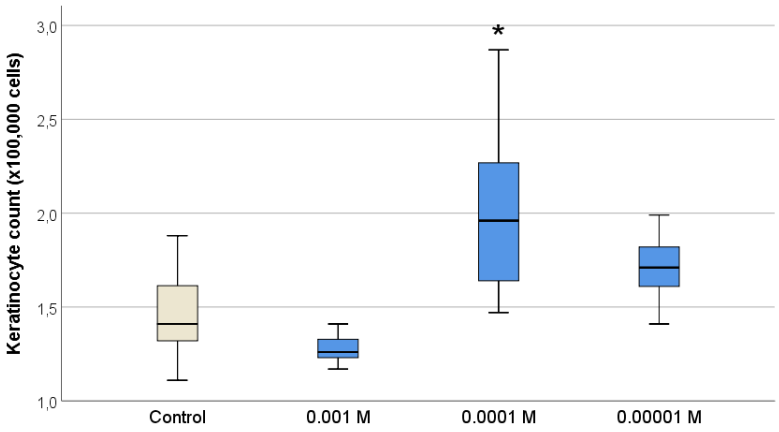

Figure 10. Effect of different concentrations of Gd_2O_3 NPs on proliferative activity of fibroblasts (HaCaT cell line) by direct cell counting using an automated cell counter (ANOVA OD:F=6.38; df3, p=0,002).

 doi:10.20944/preprints202411.1441.v1

Table 3. Descriptive statistics of the results of in-vitro studies on human keratinocyte culture when co-cultured with gadolinium oxide nanoparticles at different concentrations.

	Mean	Std. Deviation	Std. Error	95% Confidence Interval for Mean		Minimum	Maximum
				Lower	Upper		
MTT, optical density value (OD)							
Control	0.322	0.007	0.002	0.316	0.329	0.315	0.334
Gd_2O_3 (10^{-3}M)	0.335	0.011	0.004	0.324	0.345	0.322	0.351
Gd_2O_3 (10^{-4}M)	0.339	0.010	0.003	0.329	0.348	0.321	0.353
Gd_2O_3 (10^{-5}M)	0.341	0.007	0.003	0.334	0.348	0.333	0.355
Total	0.334	0.011	0.002	0.330	0.339	0.315	0.355
Number of keratinocytes, x100,000 cells							
Control	1.47	0.268	0.101	1.21	1.71	1.11	1.88
Gd_2O_3 (10^{-3}M)	1.33	0.157	0.059	1.18	1.47	1.17	1.64
Gd_2O_3 (10^{-4}M)	2.02	0.515	0.194	1.53	2.49	1.47	2.87
Gd_2O_3 (10^{-5}M)	1.71	0.192	0.072	1.53	1.89	1.41	1.99
Total	1.63	0.399	0.075	1.47	1.78	1.11	2.87

A high level of biocompatibility of the investigated concentrations of Gd_2O_3 NPs in relation to human keratinocyte culture was determined. There were no dead cells registered in any of the wells. Microscopy of keratinocytes in different groups also did not reveal any negative cytoarchitectonic changes (Figure 11).

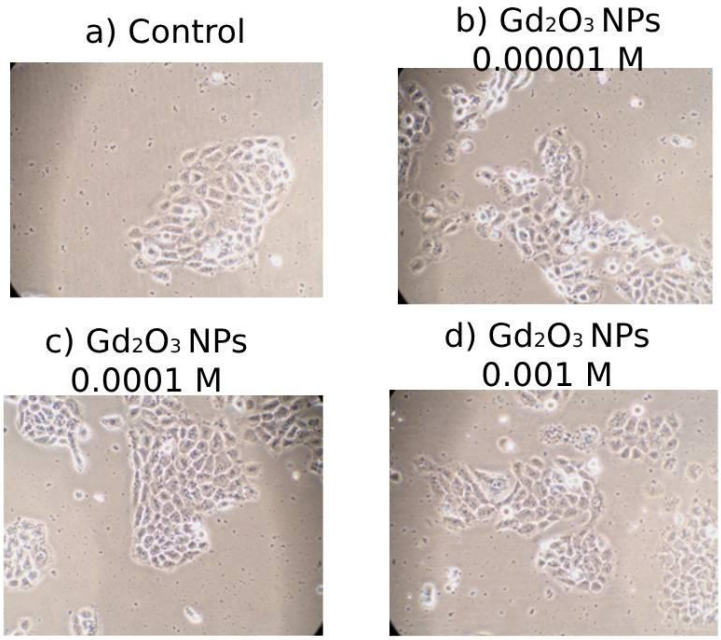

Figure 11. Human keratinocytes after 72-hour incubation with different concentrations of Gd_2O_3 NPs compared to control, magnification×20.

Thus, the revealed ability of Gd_2O_3 NPs to stimulate human keratinocytes can be the basis for further studies to develop nanomaterials based on Gd_2O_3 NPs for skin wound healing. A comprehensive analysis of the tests performed on keratinocytes allows us to choose the best concentration of 10^{-4}M for their stimulation, at which there is activation of both metabolism and proliferative activity of keratinocytes.

 doi:10.20944/preprints202411.1441.v1

3.3.3. Results of the Study of Migration Activity and Healing Rate of a Model Wound In Vitro on Human Mesenchymal Stem Cell Culture

The treatment of MSCs with Gd_2O_3 displayed distinct and heterogenic effects on wound scratch closure compared to intact MSCs (Figure 12a). Enhanced migration and more rapid scratch closure were observed in Gd_2O_3 treated MSCs compared to their untreated counterparts within 24 h. However, the scratch disappeared by the third day for both treated and resting MSCs (Figure 12b).

Surprisingly, the arrangement of cells in the scratches varied greatly. Individual cells from the untreated MSC line rapidly migrated to the center of the scratch, where they were oriented randomly. At the same time, the cell front at the edges of the scratch remained practically unchanged. In contrast, Gd_2O_3-treated MSCs hardly migrated to the center of the scratch. Overgrowth of the scratch in this case occurred due to the collective movement of leading cells. In this case, Gd_2O_3 treated MSCs lined up parallel along the scratch (Figure 12a).

These results suggest that Gd_2O_3 may not only have a stimulatory effect on scratch healing, but also determine the functional heterogeneity of MSCs.

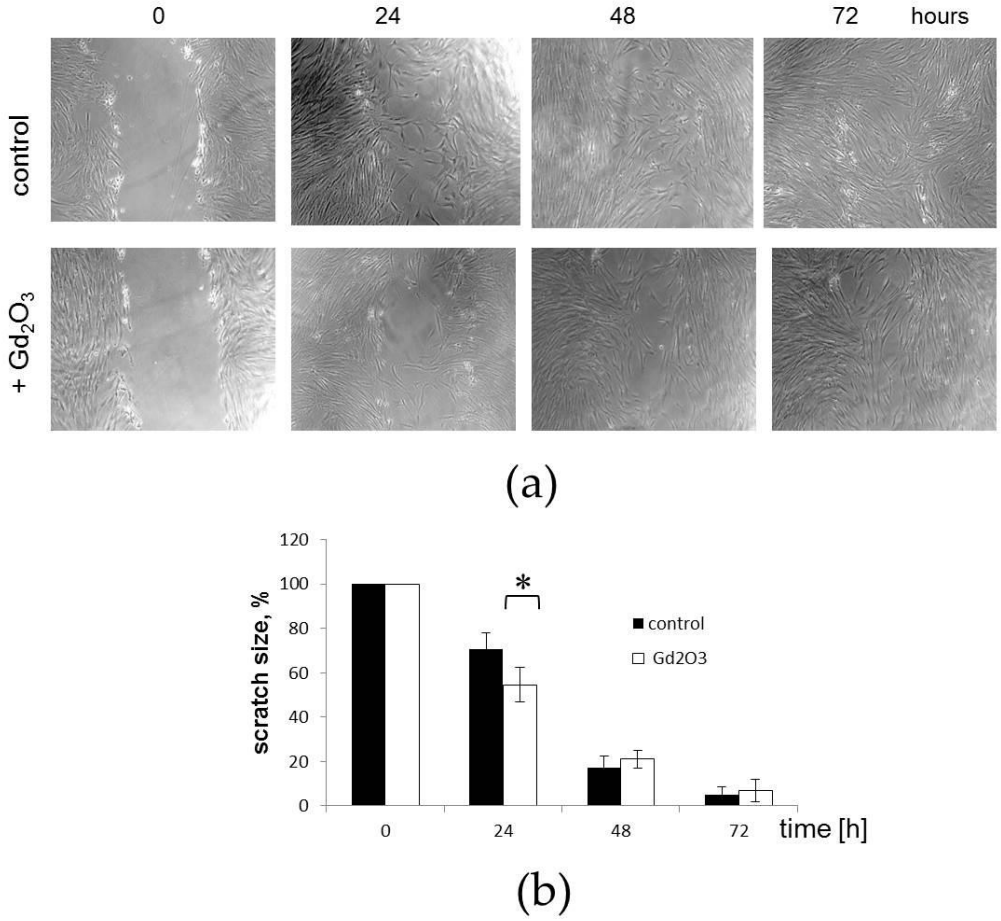

Figure 12. Effects of Gd_2O_3 on migration of MSCs in scratch wound healing assay. **(a)** Representative images demonstrate the differences in migratory activity between MSCs under intact conditions and upon the Gd2O3 treatment. Brightfield microscopy, magnification —40×. **(b)** Time-dependent quantification of % confluency in the scratch wound area (* reliability of differences at $p < 0.05$; t-test).

4. Discussion

Nanoscale gadolinium oxide (Gd_2O_3) is a promising nanomaterial with unique physicochemical properties that has various applications ranging from biomedicine to catalysis. Most of the current published studies on gadolinium compounds are related to their use as clinical contrast agents for MRI [7–12]. However, there are significant safety and toxicity problems associated with the use of nanomaterials in biomedical applications. Assessments of biocompatibility and nanotoxicology are

 doi:10.20944/preprints202411.1441.v1

important to support the safe usage of these materials [77–79]. Obtaining safer and more efficient nanoparticles for biomedical applications remains a still a challenge [80,81]. There are published single studies on the physicochemical properties of crystalline complexes of Gd_2O_3 NPs without cytotoxic effects on cellular structures [82,83]. Therefore, studies on the effects of nanosized gadolinium oxides on various cell lines over a wide range of concentrations are of significant interest.

The conducted study on systematic integrated evaluation of chemical-physical characteristics and biological action of Gd_2O_3 NPs provided interesting scientific data that may be useful for further development and potential application of Gd_2O_3 NPs nanoparticles not only for tissue visualization for diagnostic purposes, but also for therapeutic medicine.

The synthesized gadolinium oxide nanoparticles by thermal decomposition of gadolinium carbonate precipitated from nitrate solution (this method is suitable for large-scale production) had an average size of 20-30 nm and a relatively high degree of crystallinity with the structure of cubic singony and lattice parameter a = 10.79(9) Å. The spectrum obtained by Raman spectroscopy contained peaks in all three regions described above, and their position agreed well with the position of Raman active modes and those caused by the main vibrations of atoms in the crystal lattice (Gd-Gd and Gd-O) or their combinations, which spoke about the structural quality of Gd_2O_3 nanocrystals.

Thus, the analysis performed by instrumental methods confirmed both the chemical composition of the studied substance and its physicochemical characteristics, which made it possible to start studying the effect of gadolinium oxide nanoparticles on biological objects.

It was found that Gd_2O_3 NPs were highly biocompatible at a concentration of $\leq 10^{-3}$M, which was attributed to exhibiting antioxidant properties.

However, in the study on cell cultures, we did not obtain a direct correlation of the antioxidant effect to the studied concentration ranges. Nevertheless, increasing the concentration of the studied substance to the growth medium resulted in a significant increase in the proliferative activity of fibroblasts with relatively little metabolic activity. Studies on cell lines showed a high level of safety and regenerative potential of Gd_2O_3 NPs, which stimulated fibroblast metabolism at concentrations of 10^{-2} to 10^{-3}M (27-28% enhancement), i.e. they were able to enhance the production of interstitial matter during regeneration (collagen, elastin) without affecting the proliferation of human fibroblasts and demonstrating high biocompatibility. The identified ability of Gd_2O_3 NPs to stimulate human keratinocytes may be the basis for further research to develop nanomaterials based on Gd_2O_3 NPs for skin wound healing. Complex analysis of the tests performed on keratinocytes allows choosing the best concentration of 10^{-4}M for their stimulation, at which there is activation of both metabolism and proliferative activity of keratinocytes (cell growth is enhanced on average by 37% at the concentration of 10^{-4}M). Lower and higher concentrations of gadolinium nanoparticles (10^{-3}M and 10^{-5}M) did not enhance proliferation growth, on the contrary, at the concentration of 10^{-3}M an unreliable tendency to decrease the growth of keratinocyte cell number was determined.

The obtained data demonstrate the pharmacologic potential of nanogadolinium in wound healing agents. Tissue regeneration is impossible without the participation of multipotent mesenchymal stromal cells (MSCs), as they perform a regulatory function at the site of injury, stimulating cell recruitment, angiogenesis, synthesis and remodeling of extracellular matrix. In particular, it has been shown that MSCs contribute to the reduction of inflammation and promote successful healing through dynamically changing secretion of cytokines, chemokines, growth factors, extracellular vesicles and extracellular matrix proteins under the influence of external signals from the microenvironment [84,85]. The obtained data from studies on MSCs with regard to the ability of Gd_2O_3 NPs not only to accelerate scratch healing but also to determine the functional heterogeneity of MSCs may bring beneficial effects in regenerative meditine not only for skin wound healing but also for reparative processes of internal organs.

Structural defects, which are detected by the results of studies, being located on the surface of nanoparticles, can perform a functional role as centers on which the uncompensated charge is localized and on which redox reactions can take place. Consequently, the increase of structural defects on the surface can lead to the growth of redox-active centers and increase the chemical activity of nanoparticles.

 doi:10.20944/preprints202411.1441.v1

In our case, increasing the concentration to 10^{-2} M did not reveal such an effect. However, the effect could be reduced due to the strong agglomeration of nanoparticles noted during culture studies, which could reduce the number of working active centers. This further emphasizes the need for measures to reduce agglomeration of nanoparticles in solutions when developing medical devices. This problem is usually solved by immersing the nanoparticle in a polymer, carbronic acid or polysaccharide to create a thin coating. In our case, when the primary aim was to study the physical parameters of the nanoparticle, we used uncoated nanogadolinium. In addition, the toxic effects of the uncoated particle could be stronger, and the study of this was our second aim.

It is worth noting that under light irradiation, the reason for the simultaneous pro- and antioxidant activity may have been due to a different mechanism. The nonlinear dependence of the redox effect can be explained by an up-conversion mechanism characteristic of $Gd_2O_3:Eu^{3+}$ compounds. Apparently, at high concentrations of Gd_2O_3 NPs, the prooxidant effect may prevail over antioxidant processes, but further studies are required to prove and study these mechanisms.

According to Raman spectroscopy and EDX analysis, the structure of Gd_2O_3 NPs contains insignificant amounts of impurities that can cause the manifestation of prooxidant properties when the particles are irradiated with red light. But, firstly, the amount of these impurities was small, and we did not find any signs indicating the resulting toxic effects during the studies in cell cultures. Second, the presence of lanthanide impurities can enhance the luminescent properties of Gd_2O_3 NPs, which directly depend on the additional impurity energy levels inside the forbidden band Gd_2O_3. It is known that Gd_2O_3 doped with impurity elements (Eu, Yb, etc.) is a pronounced up-conversion luminophore [86], which is able to excite electron-hole pairs, including luminescent ones, due to multiphoton absorption of low-energy light quanta. In this case, electron-hole pairs can be separated by an energy barrier exceeding the energy of single photons of the excitation radiation. The concentration of impurity elements can be rather low, nevertheless providing high quantum yield. When Gd_2O_3 NPs are irradiated with red light photons, the photogenerated electron-hole pairs with long lifetime can migrate to the particle surface and initiate a cascade of redox reactions accompanied by the release of active radicals [87]. It appears that at high concentrations of Gd_2O_3 NPs, pro-oxidant effects may prevail over antioxidant processes, but further studies are required to prove and explore these mechanisms. This can be and, obviously, will be used in imaging systems in our studies on the distribution and excretion of gadolinium oxide nanoparticles from the animal organism at different methods of its administration (percutaneous, oral, injection, injection into the vascular bed). Conducting lifetime tagging studies will help us answer some of the questions of drug delivery and, hopefully, cancer treatment.

At this stage our work has shown biocompatibility (absence of cytotoxic effects) of Gd_2O_3 NPs in concentrations 10^{-2}M -10^{-5}M on different cell lines involved in wound regeneration: MSCs, fibroblasts, keratinocytes. The best effect was found when co-culturing with Gd_2O_3 NPs in concentrations 10^{-4}M, when in 24h the directed migration of MSCs was significantly increased, and in 72h the proliferation of keratinocytes was enhanced, which is very useful in regeneration, including in skin wound healing.

5. Conclusions

1. The method of thermal decomposition of gadolinium carbonate used for the preparation of nanosized gadolinium (III) oxide is suitable for large-scale production and results in obtaining high chemical purity Gd_2O_3 NPs of cubic structure with an average size of 20-30 nm, and the particles have a relatively high degree of crystallinity.
2. In the study of photooxidative degradation of methylene blue dye in the presence of Gd_2O_3 NPs under red light irradiation, it was found that Gd_2O_3 nanoparticles showed weakly pronounced antioxidant activity, which depends on the content of particles in the solution. At a concentration of 10^{-3}M, the highest antioxidant activity of Gd_2O_3 nanoparticles is observed when the rate constant of the dye photodegradation reaction decreases by 5.5% to $9.4x10^{-3}$ min^{-1}. When the concentration of Gd_2O_3 NPs in solution is increased to 10^{-2}M upon irradiation with a red light

 doi:10.20944/preprints202411.1441.v1

source, their antioxidant activity changes to pro-oxidant activity, accompanied by a 15% increase in the rate of the methylene blue degradation reaction.

3. Studies on cell lines showed a high level of safety and regenerative potential of Gd_2O_3 NPs, which stimulated fibroblast metabolism at concentrations of 10^{-2} to 10^{-3}M (27% enhancement) without affecting their proliferation. Gd_2O^3 NPs stimulated keratinocyte metabolism at concentrations of 10^{-3}M-10^{-6}M, and enhanced keratinocyte proliferation by an average of 35% at concentrations of 10^{-4}M. Gd_2O^3 NPs accelerated the migration of MSCs, enhancing their proliferation, promoting the healing of the model wound.

Thus, the results of this study demonstrated the safety and high regenerative potential of redox-active Gd_2O_3 NPs nanoparticles towards different cell lines involved in wound regeneration. This may be the basis for further research to develop nanomaterials based on Gd_2O_3 NPs for skin wound healing and in regenerative medicine generally. Comprehensive analysis allows the selection of 10^{-4}M concentration for the development of a drug for wound healing.

Author Contributions: Conceptualization, E.V.S., V.A.S. and N.E.M.; methodology, E.V.S., E.L.C., M.A.P. and, Y.G.S.; validation, A.A.K. and A.A.K.; investigation, E.L.C., A.A.G., A.A.K., O.I.A., Y.G.S., M.A.P. and A.V.K.; formal analysis, A.A.K., N.E.M. and V.A.S.; data curation, E.L.C., Y.G.S. and E.V.S.; visualization, V.A.S.. E.V.S., A.A.G., Y.G.S. M.A.P. and A.V.K.; supervision, E.V.S., N.E.M. and V.A.S.; project administration, E.V.S.; writing—original draft preparation, E.V.S., V.A.S., O.I.A., A.A.K., and M.A.P. writing—review and editing, E.L.C., A.A.G., Y.G.S., A.V.K. and N.E.M. All authors have read and agreed to the published version of the manuscript.

Funding: The work was carried out with the support of the I.M. Sechenov First Moscow State Medical University (Sechenov University) development program project "Possibilities of biomedical application of rare earth metal compounds", project code 04.000.y.128.

Informed Consent Statement: Not applicable, the study did not involve humans.

Data Availability Statement: Details regarding the data supporting the reported results can be found from the first authors.

Conflicts of Interest: The authors declare no conflicts of interest. The funder (Sechenov University) was not involved in the study's design, and did not affect its results. The «LANHIT» company, established by the State Institute of Rare Earth Metallurgy of the Russian Academy of Sciences, which carried out the synthesis of NPs, did not sponsor this study and did not participate in the further instrumental analysis of the obtained materials that were not performed on the basis of LANHIT.

References

1. Eilers A, Witt S, Walter J. Aptamer-Modified Nanoparticles in Medical Applications. Adv Biochem Eng Biotechnol. 2020;174:161-193. doi: 10.1007/10_2020_124.
2. Najahi-Missaoui W, Arnold RD, Cummings BS. Safe Nanoparticles: Are We There Yet? Int J Mol Sci. 2020 Dec 31;22(1):385. doi: 10.3390/ijms22010385.
3. Wen J, Moloney EB, Canning A, Donohoe E, Ritter T, Wang J, Xiang D, Wu J, Li Y. Synthesized nanoparticles, biomimetic nanoparticles and extracellular vesicles for treatment of autoimmune disease: Comparison and prospect. Pharmacol Res. 2021 Oct;172:105833. doi: 10.1016/j.phrs.2021.105833.
4. Ali M. What function of nanoparticles is the primary factor for their hyper-toxicity? Adv Colloid Interface Sci. 2023 Apr;314:102881. doi: 10.1016/j.cis.2023.102881.
5. Hendricks AR, Guilliams BF, Cohen RS, Tien T, McEwen GA, Borgognoni KM, Ackerson CJ. Cloneable inorganic nanoparticles. Chem Commun (Camb). 2023 Jul 11;59(56):8626-8643. doi: 10.1039/d3cc01319g.
6. Medical Advisory Secretariat. Nanotechnology: an evidence-based analysis. Ont Health Technol Assess Ser. 2006;6(19):1-43. Epub 2006 Nov 1. PMID: 23074489; PMCID: PMC3379172
7. Dai Y, Wu C, Wang S, Li Q, Zhang M, Li J, Xu K. Comparative study on in vivo behavior of PEGylated gadolinium oxide nanoparticles and Magnevist as MRI contrast agent. Nanomedicine. 2018 Feb;14(2):547-555. doi: 10.1016/j.nano.2017.12.005.
8. Wallnöfer EA, Thurner GC, Kremser C, Talasz H, Stollenwerk MM, Helbok A, Klammsteiner N, Albrecht-Schgoer K, Dietrich H, Jaschke W, Debbage P. Albumin-based nanoparticles as contrast medium for MRI:

vascular imaging, tissue and cell interactions, and pharmacokinetics of second-generation nanoparticles. Histochem Cell Biol. 2021 Jan;155(1):19-73. doi: 10.1007/s00418-020-01919-0.

9. Wu L, Lu X, Lu Y, Shi M, Guo S, Feng J, Yang S, Xiong W, Xu Y, Yan C, Shen Z. Kilogram-Scale Synthesis of Extremely Small Gadolinium Oxide Nanoparticles as a T1-Weighted Contrast Agent for Magnetic Resonance Imaging. Small. 2024 Apr;20(14):e2308547. doi: 10.1002/smll.202308547.
10. Liu K, Cai Z, Chi X, Kang B, Fu S, Luo X, Lin ZW, Ai H, Gao J, Lin H. Photoinduced Superhydrophilicity of Gd-Doped TiO2 Ellipsoidal Nanoparticles Boosts *T*1 Contrast Enhancement for Magnetic Resonance Imaging. Nano Lett. 2022 Apr 27;22(8):3219-3227. doi: 10.1021/acs.nanolett.1c04676.
11. Riyahi-Alam, N.; Behrouzkia, Z.; Seifalian, A.; HaghgooJahromi, S. Properties Evaluation of a New MRI Contrast Agent Based on Gd-Loaded Nanoparticles. Biol. Trace Elem. Res. 2010, 137, 324–334, doi:10.1007/s12011-009-8587-3.
12. Caravan P, Ellison JJ, McMurry TJ, Lauffer RB. Gadolinium(III) chelates as MRI contrast agents: structure, dynamics, and applications. Chem Rev. 1999;99:2293–3235. doi: 10.1021/cr980440x.
13. Helm L. Optimization of gadolinium-based MRI contrast agents for high magnetic-field applications. Future Med Chem. 2010;2:385–396. doi: 10.4155/FMC.09.174.
14. Fleming CL, Wong J, Golzan M, Gunawan C, McGrath KC. Insights from a Bibliometrics-Based Analysis of Publishing and Research Trends on Cerium Oxide from 1990 to 2020. Int J Mol Sci. 2023 Jan 20;24(3):2048. doi: 10.3390/ijms24032048.
15. Farias IAP, Dos Santos CCL, Sampaio FC. Antimicrobial Activity of Cerium Oxide Nanoparticles on Opportunistic Microorganisms: A Systematic Review. Biomed Res Int. 2018 Jan 23;2018:1923606. doi: 10.1155/2018/1923606.
16. Xue Y, Yang F, Wu L, Xia D, Liu Y. CeO2 Nanoparticles to Promote Wound Healing: A Systematic Review. Adv Healthc Mater. 2024 Mar;13(6):e2302858. doi: 10.1002/adhm.202302858.
17. Silina E.V., Manturova N.E., Erokhina A.G., Shatokhina E.A., Stupin V.A. Nanomaterials based on cerium oxide nanoparticles for wound regeneration: a literature review. *Russian Journal of Transplantology and Artificial Organs*. 2024;26(1):113-124. https://doi.org/10.15825/1995-1191-2024-1-113-124
18. Rajaee A, Wang S, Zhao L, Wang D, Liu Y, Wang J, Ying K. Multifunction bismuth gadolinium oxide nanoparticles as radiosensitizer in radiation therapy and imaging. Phys Med Biol. 2019 Oct 4;64(19):195007. doi: 10.1088/1361-6560/ab2154.
19. Lux F, Sancey L, Bianchi A, Crémillieux Y, Roux S, Tillement O. Gadolinium-based nanoparticles for theranostic MRI-radiosensitization. Nanomedicine (Lond). 2015;10(11):1801-15. doi: 10.2217/nnm.15.30.
20. Liu W, Deacon J, Yan H, Sun B, Liu Y, Hegan D, Li Q, Coman D, Parent M, Hyder F, Roberts K, Nath R, Tillement O, Engelman D, Glazer P. Tumor-targeted pH-low insertion peptide delivery of theranostic gadolinium nanoparticles for image-guided nanoparticle-enhanced radiation therapy. Transl Oncol. 2020 Nov;13(11):100839. doi: 10.1016/j.tranon.2020.100839.
21. Khorasani A, Shahbazi-Gahrouei D, Safari A. Recent Metal Nanotheranostics for Cancer Diagnosis and Therapy: A Review. Diagnostics (Basel). 2023 Feb 22;13(5):833. doi: 10.3390/diagnostics13050833.
22. Zhang J, Su X, Weng L, Tang K, Miao Y, Teng Z, Wang L. Gadolinium-hybridized mesoporous organosilica nanoparticles with high magnetic resonance imaging performance for targeted drug delivery. J Colloid Interface Sci. 2023 Mar;633:102-112. doi: 10.1016/j.jcis.2022.11.085.
23. Ho SL, Choi G, Yue H, Kim HK, Jung KH, Park JA, Kim MH, Lee YJ, Kim JY, Miao X, Ahmad MY, Marasini S, Ghazanfari A, Liu S, Chae KS, Chang Y, Lee GH. *In vivo* neutron capture therapy of cancer using ultrasmall gadolinium oxide nanoparticles with cancer-targeting ability. RSC Adv. 2020 Jan 3;10(2):865-874. doi: 10.1039/c9ra08961f.
24. Zhou T, Zhang S, Zhang L, Jiang T, Wang H, Huang L, Wu H, Fan Z, Jing S. Redox ferrocenylseleno compounds modulate longitudinal and transverse relaxation times of FNPs-Gd MRI contrast agents for multimodal imaging and photo-Fenton therapy. Acta Biomater. 2023 Jul 1;164:496-510. doi: 10.1016/j.actbio.2023.04.006.
25. Pan J , Zhu X , Chen X , Zhao Y , Liu J . Gd3+-Doped MoSe2 nanosheets used as a theranostic agent for bimodal imaging and highly efficient photothermal cancer therapy. Biomater Sci. 2018 Jan 30;6(2):372-387. doi: 10.1039/c7bm00894e.
26. Jin S, Zhou L, Gu Z, Tian G, Yan L, Ren W, Yin W, Liu X, Zhang X, Hu Z, Zhao Y. A new near infrared photosensitizing nanoplatform containing blue-emitting up-conversion nanoparticles and hypocrellin A for photodynamic therapy of cancer cells. Nanoscale. 2013 Dec 7;5(23):11910-8. doi: 10.1039/c3nr03515h.

27. Wang J, Sun X, Xu J, Liu L, Lin P, Luo X, Gao Y, Shi J, Zhang Y. X-ray activated near-infrared persistent luminescence nanoparticles for trimodality *in vivo* imaging. Biomater Sci. 2024 Jul 23;12(15):3841-3850. doi: 10.1039/d4bm00395k.
28. Chargari C, Maury P, Texier M, Genestie C, Morice P, Bockel S, Gouy S, Ba M, Achkar S, Lux F, Tillement O, Dufort S, Duc GLE, Debeaumont O, Massard C, Maulard A, Porcel E, Bahleda R, Ammari S, Morel D, Espenel S, Pautier P, Robert C, Deutsch E. Theragnostic Gadolinium-Based Nanoparticles Safely Augment X-ray Radiation Effects in Patients with Cervical Cancer. ACS Nano. 2024 Jul 2;18(26):16516-16529. doi: 10.1021/acsnano.3c12537.
29. Yu B, Lu X, Feng X, Zhao T, Li J, Lu Y, Ye F, Liu X, Zheng X, Shen Z, Jin X, Chen W, Li Q. Gadolinium Oxide Nanoparticles Reinforce the Fractionated Radiotherapy-Induced Immune Response in Tri-Negative Breast Cancer via cGAS-STING Pathway. Int J Nanomedicine. 2023 Dec 15;18:7713-7728. doi: 10.2147/IJN.S428044.
30. Hu P, Fu Z, Liu G, Tan H, Xiao J, Shi H, Cheng D. Gadolinium-Based Nanoparticles for Theranostic MRI-Guided Radiosensitization in Hepatocellular Carcinoma. Front Bioeng Biotechnol. 2019 Nov 27;7:368. doi: 10.3389/fbioe.2019.00368.
31. Nosrati H, Salehiabar M, Charmi J, Yaray K, Ghaffarlou M, Balcioglu E, Ertas YN. Enhanced In Vivo Radiotherapy of Breast Cancer Using Gadolinium Oxide and Gold Hybrid Nanoparticles. ACS Appl Bio Mater. 2023 Feb 20;6(2):784-792. doi: 10.1021/acsabm.2c00965.
32. Korolev DV, Shulmeyster GA, Istomina MS, Evreinova NV, Aleksandrov IV, Krasichkov AS, Postnov VN, Galagudza MM. Fluorescently Labeled Gadolinium Ferrate/Trigadolinium Pentairon(III) Oxide Nanoparticles: Synthesis, Characterization, In Vivo Biodistribution, and Application for Visualization of Myocardial Ischemia-Reperfusion Injury. Materials (Basel). 2022 May 27;15(11):3832. doi: 10.3390/ma15113832.
33. Almas T, Haider R, Malik J, Mehmood A, Alvi A, Naz H, Satti DI, Zaidi SMJ, AlSubai AK, AlNajdi S, Alsufyani R, Ramtohul RK, Almesri A, Alsufyani M, H Al-Bunnia A, Alghamdi HAS, Sattar Y, Alraies MC, Raina S. Nanotechnology in interventional cardiology: A state-of-the-art review. Int J Cardiol Heart Vasc. 2022 Nov 18;43:101149. doi: 10.1016/j.ijcha.2022.101149.
34. Lee H, Choi SH, Anzai Y. Glymphatic MRI techniques in sleep and neurodegenerative diseases. Curr Opin Pulm Med. 2022 Nov 1;28(6):499-510. doi: 10.1097/MCP.0000000000000923.
35. Lilius TO, Mortensen KN, Deville C, Lohela TJ, Stæger FF, Sigurdsson B, Fiordaliso EM, Rosenholm M, Kamphuis C, Beekman FJ, Jensen AI, Nedergaard M. Glymphatic-assisted perivascular brain delivery of intrathecal small gold nanoparticles. J Control Release. 2023 Mar;355:135-148. doi: 10.1016/j.jconrel.2023.01.054.
36. Lu R, Zhang Y, Tao H, Zhou L, Li H, Chen T, Zhang P, Lu Y, Chen S. Gadolinium-hyaluronic acid nanoparticles as an efficient and safe magnetic resonance imaging contrast agent for articular cartilage injury detection. Bioact Mater. 2020 Jun 21;5(4):758-767. doi: 10.1016/j.bioactmat.2020.05.009.
37. Wu S, Xu T, Gao J, Zhang Q, Huang Y, Liu Z, Hao X, Yao Z, Hao X, Wu PY, Wu Y, Yin B, Tang Z. Non-invasive diagnosis of liver fibrosis via MRI using targeted gadolinium-based nanoparticles. Eur J Nucl Med Mol Imaging. 2024 Sep 5. doi: 10.1007/s00259-024-06894-5.
38. Brune N, Mues B, Buhl EM, Hintzen KW, Jockenhoevel S, Cornelissen CG, Slabu I, Thiebes AL. Dual Labeling of Primary Cells with Fluorescent Gadolinium Oxide Nanoparticles. Nanomaterials (Basel). 2023 Jun 16;13(12):1869. doi: 10.3390/nano13121869.
39. Mehta KJ. Iron Oxide Nanoparticles in Mesenchymal Stem Cell Detection and Therapy. Stem Cell Rev Rep. 2022 Oct;18(7):2234-2261. doi: 10.1007/s12015-022-10343-x.
40. Yu T , Zhen M , Li J , Zhou Y , Ma H , Jia W , Wang C . Anti-apoptosis effect of amino acid modified gadofullerene via a mitochondria mediated pathway. Dalton Trans. 2019 Jun 14;48(22):7884-7890. doi: 10.1039/c9dt00800d.
41. Wang J, Chen C, Li B, Yu H, Zhao Y, Sun J, Li Y, Xing G, Yuan H, Tang J, Chen Z, Meng H, Gao Y, Ye C, Chai Z, Zhu C, Ma B, Fang X, Wan L. Antioxidative function and biodistribution of [Gd@C82(OH)22]n nanoparticles in tumor-bearing mice. Biochem Pharmacol. 2006 Mar 14;71(6):872-81. doi: 10.1016/j.bcp.2005.12.001.
42. Jiao F, Qu Y, Zhou G, Liu Y, Li W, Ge C, Li Y, Hu W, Li B, Gao Y, Chen C. Modulation of oxidative stress by functionalized fullerene materials in the lung tissues of female C57/BL mice with a metastatic Lewis lung carcinoma. J Nanosci Nanotechnol. 2010 Dec;10(12):8632-7. doi: 10.1166/jnn.2010.2489.

43. Maksimchuk PO, Hubenko KO, Seminko VV, Karbivskii VL, Tkachenko AS, Onishchenko AI, Prokopyuk VY, Yefimova SL. High antioxidant activity of gadolinium-yttrium orthovanadate nanoparticles in cell-free and biological milieu. Nanotechnology. 2021 Nov 8;33(5). doi: 10.1088/1361-6528/ac31e5.
44. Sushko ES, Vnukova NG, Churilov GN, Kudryasheva NS. Endohedral Gd-Containing Fullerenol: Toxicity, Antioxidant Activity, and Regulation of Reactive Oxygen Species in Cellular and Enzymatic Systems. Int J Mol Sci. 2022 May 5;23(9):5152. doi: 10.3390/ijms23095152.
45. Luo S, Ma D, Wei R, Yao W, Pang X, Wang Y, Xu X, Wei X, Guo Y, Jiang X, Yuan Y, Yang R. A tumor microenvironment responsive nanoplatform with oxidative stress amplification for effective MRI-based visual tumor ferroptosis. Acta Biomater. 2022 Jan 15;138:518-527. doi: 10.1016/j.actbio.2021.11.007..
46. Kollef MH, Torres A, Shorr AF, Martin-Loeches I, Micek ST. Nosocomial Infection. Crit Care Med. 2021 Feb 1;49(2):169-187. doi: 10.1097/CCM.0000000000004783.
47. Ji B, Ye W. Prevention and control of hospital-acquired infections with multidrug-resistant organism: A review. Medicine (Baltimore). 2024 Jan 26;103(4):e37018. doi: 10.1097/MD.0000000000037018.
48. Flynn CE, Guarner J. Emerging Antimicrobial Resistance. Mod Pathol. 2023 Sep;36(9):100249. doi: 10.1016/j.modpat.2023.100249. Epub 2023 Jun 21. PMID: 37353202.
49. Lemiech-Mirowska E, Kiersnowska ZM, Michałkiewicz M, Depta A, Marczak M. Nosocomial infections as one of the most important problems of healthcare system. Ann Agric Environ Med. 2021 Sep 16;28(3):361-366. doi: 10.26444/aaem/122629. Epub 2020 Jun 5. PMID: 34558254.
50. Aashima, Pandey SK, Singh S, Mehta SK. Biocompatible gadolinium oxide nanoparticles as efficient agent against pathogenic bacteria. J Colloid Interface Sci. 2018 Nov 1;529:496-504. doi: 10.1016/j.jcis.2018.06.030.
51. Mohsin MH, Khashan KS, Sulaiman GM, Mohammed HA, Qureshi KA, Aspatwar A. A novel facile synthesis of metal nitride@metal oxide (BN/Gd2O3) nanocomposite and their antibacterial and anticancer activities. Sci Rep. 2023 Dec 20;13(1):22749. doi: 10.1038/s41598-023-49895-4.
52. Kumar S, Chaudhary S,, Ganga Ram Chaudhary G.R. Effect of fabrication strategies on the in-vitro antimicrobial and antifungal activities of Pr3+ doped Gb2O3 nanoparticles, Environmental Nanotechnology, Monitoring & Management, Volume 16, 2021, 100518, ISSN 2215-1532, https://doi.org/10.1016/j.enmm.2021.100518.
53. Jin J, Zhao Q. Engineering nanoparticles to reprogram radiotherapy and immunotherapy: recent advances and future challenges. J Nanobiotechnology. 2020 May 14;18(1):75. doi: 10.1186/s12951-020-00629-y.
54. Ahmad MY, Ahmad MW, Yue H, Ho SL, Cha H, Marasini S, Tegafaw T, Liu S, Ghazanfari A, Chae KS, Chang Y, Lee GH. Chitosan Oligosaccharide Lactate-Coated Ultrasmall Gadolinium Oxide Nanoparticles: Synthesis, *In Vitro* Cytotoxicity, and Relaxometric Properties. J Nanosci Nanotechnol. 2021 Aug 1;21(8):4145-4150. doi: 10.1166/jnn.2021.19378.
55. Liu S, Yue H, Ho SL, Kim S, Park JA, Tegafaw T, Ahmad MY, Kim S, Saidi AKAA, Zhao D, Liu Y, Nam SW, Chae KS, Chang Y, Lee GH. Enhanced Tumor Imaging Using Glucosamine-Conjugated Polyacrylic Acid-Coated Ultrasmall Gadolinium Oxide Nanoparticles in Magnetic Resonance Imaging. Int J Mol Sci. 2022 Feb 4;23(3):1792. doi: 10.3390/ijms23031792.
56. Tamanoi F, Yoshikawa K. Inhibition of DNA synthesis and cancer therapies. Enzymes. 2022;52:11-21. doi: 10.1016/bs.enz.2022.10.002.
57. Wallnöfer EA, Thurner GC, Kremser C, Talasz H, Stollenwerk MM, Helbok A, Klammsteiner N, Albrecht-Schgoer K, Dietrich H, Jaschke W, Debbage P. Albumin-based nanoparticles as contrast medium for MRI: vascular imaging, tissue and cell interactions, and pharmacokinetics of second-generation nanoparticles. Histochem Cell Biol. 2021 Jan;155(1):19-73. doi: 10.1007/s00418-020-01919-0.
58. Kraus W., Nolze G.. Powder cell - a program for the representation and manipulation of crystal structures and calculation of the resulting X-ray powder patterns J. Appl. Cryst. 1996. 29. 301-303.
59. Artini, C., Costa, G. A., Pani, M., Lausi, A., Plaisier, J. Structural characterization of the CeO2/Gd2O3 mixed system by synchrotron X-ray diffraction. Journal of Solid State Chemistry, 2012. 190, 24–28. doi:10.1016/j.jssc.2012.01.056
60. Wilson VG. Growth and differentiation of HaCaT keratinocytes. Methods Mol Biol. 2014;1195:33-41. doi: 10.1007/7651_2013_42.
61. Colombo I, Sangiovanni E, Maggio R, Mattozzi C, Zava S, Corbett Y, Fumagalli M, Carlino C, Corsetto PA, Scaccabarozzi D, Calvieri S, Gismondi A, Taramelli D, Dell'Agli M. HaCaT Cells as a Reliable In Vitro Differentiation Model to Dissect the Inflammatory/Repair Response of Human Keratinocytes. MediatorsInflamm. 2017;2017:7435621. doi: 10.1155/2017/7435621

62. Suzdaltseva Y, Goryunov K, Silina E, Manturova N, Stupin V, Kiselev SL. Equilibrium among Inflammatory Factors Determines Human MSC-Mediated Immunosuppressive Effect. Cells. 2022 Apr 3;11(7):1210. doi: 10.3390/cells11071210
63. Dominici M, Le Blanc K, Mueller I, Slaper-Cortenbach I, Marini F, Krause D, Deans R, Keating A, Prockop Dj, Horwitz E. Minimal criteria for defining multipotent mesenchymal stromal cells. The International Society for Cellular Therapy position statement. Cytotherapy. 2006;8(4):315-7. doi: 10.1080/14653240600855905.
64. Pires, A.M.; Davolos, M.R.; Paiva-Santos, C.O.; Stucchi, E.B.; Flor, J. New X-Ray Powder Diffraction Data and Rietveld Refinement for Gd 2 O 3 Monodispersed Fine Spherical Particles. J. Solid State Chem. 2003, 171, 420–423, doi:10.1016/S0022-4596(02)00224-4.
65. Langford, J.I.; Wilson, A.J.C. Scherrer after Sixty Years: A Survey and Some New Results in the Determination of Crystallite Size. J. Appl. Crystallogr. 1978, 11, 102–113, doi:10.1107/S0021889878012844
66. Kislov, A.N.; Zatsepin, A.F. Defect Structure and Vibrational States in Eu-Doped Cubic Gadolinium Oxide. Phys. Chem. Chem. Phys. 2020, 22, 24498–24505, doi:10.1039/D0CP04281A.
67. Vairapperumal, T.; Pattnaik, S.; Rai, V.K.; Subramanian, B. Structural and Lattice Dynamics Investigation of Double Luminescent Nanosized Hybrid Gd2O3. Mater. Today Commun. 2023, 36, 106500, doi:10.1016/j.mtcomm.2023.106500.
68. Jegadeesan, P.; Sen, S.; Padmaprabu, C.; Srivastava, S.K.; Das, A.; Amirthapandian, S. Morphological and Optical Investigations on Gd2O3 Nanostructures. Inorg. Chem. Commun. 2023, 150, 110493, doi:10.1016/j.inoche.2023.110493.
69. Le Luyer, C.; García-Murillo, A.; Bernstein, E.; Mugnier, J. Waveguide Raman Spectroscopy of Sol–Gel Gd 2 O 3 Thin Films. J. Raman Spectrosc. 2003, 34, 234–239, doi:10.1002/jrs.980.
70. Dhananjaya, N.; Nagabhushana, H.; Nagabhushana, B.M.; Rudraswamy, B.; Sharma, S.C.; Sunitha, D.V.; Shivakumara, C.; Chakradhar, R.P.S. Effect of Different Fuels on Structural, Thermo and Photoluminescent Properties of Gd2O3 Nanoparticles. Spectrochim. Acta Part A Mol. Biomol. Spectrosc. 2012, 96, 532–540, doi:10.1016/j.saa.2012.04.067.
71. GarcíaRamírez, V.M.; García Murillo, A.; Carrillo Romo, F. de J.; Alvarez González, R.I.; Madrigal Bujaidar, E. A New Ultrafine Luminescent La2O3:Eu3+ Aerogel. Gels 2023, 9, 615, doi:10.3390/gels9080615.
72. Wakefield, G.; Holland, E.; Dobson, P.J.; Hutchison, J.L. Luminescence Properties of Nanocrystalline Y2O3:Eu. Adv. Mater. 2001, 13, 1557, doi:10.1002/1521-4095(200110)13:20<1557::AID-ADMA1557>3.0.CO;2-W.
73. Guo, H.; Dong, N.; Yin, M.; Zhang, W.; Lou, L.; Xia, S. Visible Upconversion in Rare Earth Ion-Doped Gd2O3 Nanocrystals. J. Phys. Chem. B 2004, 108, 19205–19209, doi:10.1021/jp048072q.
74. Maalej, N.M.; Qurashi, A.; Assadi, A.A.; Maalej, R.; Shaikh, M.N.; Ilyas, M.; Gondal, M.A. Synthesis of Gd2O3:EuNanoplatelets for MRI and Fluorescence Imaging. Nanoscale Res. Lett. 2015, 10, 215, doi:10.1186/s11671-015-0905-4.
75. Kostova, I.; Traykova, M.; Rastogi, V. New Lanthanide Complexes with Antioxidant Activity. Med. Chem. (Los. Angeles). 2008, 4, 371–378, doi:10.2174/157340608784872181.
76. Pugachevskii, M.A.; Rasseko, D.S.; Stupin, V.A.; Manturova, N.E.; Artyushkova, E.B.; Silina, E.V. Effect of CeO2 Nanoparticles on Hydroxyl Radicals in EPR Studies of the Photodegradation of Methylene Blue under Influence of Red Light. J. Mol. Liq. 2024, 404, 124946, doi:10.1016/j.molliq.2024.124946
77. Islam M.T., Tsnobiladze V. The Application, Safety, and Recent Developments of Commonly Used Gadolinium-Based Contrast Agents in MRI: A Scoping Review. EMJ. 2024;9[3]:63-73. https://doi.org/10.33590/emj/ZRVN2069
78. Coimbra S., Rocha S., Sousa N.R., Catarino C., Belo L., Bronze-da-Rocha E., Valente M.J., Santos-Silva A. Toxicity Mechanisms of Gadolinium and Gadolinium-Based Contrast Agents —A Review. *Int. J. Mol. Sci.*2024, *25*(7), 4071; https://doi.org/10.3390/ijms25074071
79. Arino T, Faulkner D, Bustillo KC, An DD, Jorgens D, Hébert S, McKinley C, Proctor M, Loguinov A, Vulpe C, Abergel RJ. Electron microscopy evidence of gadolinium toxicity being mediated through cytoplasmic membrane dysregulation. Metallomics. 2024 Oct 4;16(10):mfae042. doi: 10.1093/mtomcs/mfae042.
80. Wang, W., Song, S., Liu, W. et al. Two-photon excited luminescence of structural light enhancement in subwavelength SiO2 coating europium ion-doped paramagnetic gadolinium oxide nanoparticle and application for magnetic resonance imaging. Discover Nano18, 85 (2023). https://doi.org/10.1186/s11671-023-03864-y

81. Whba F., Mohamed F., Idris M. Evaluation of physicochemical and biocompatibility characteristics of gadolinium oxide nanoparticles as magnetic resonance imaging contrast agents. Radiation Physics and Chemistry, 2023;2013: 111189 https://doi.org/10.1016/j.radphyschem.2023.111189
82. Verma V.K, Srivastava P., Sabbarwal S, Singh M., Koch B., Kumar M. White Light Emitting Gadolinium Oxide Nanoclusters for In-vitro Bio-imaging, *ChemistrySelect.* 2022; 47(7): e202202335,https://doi.org/10.1002/slct.202202335
83. Zheng C, Tian X, Cai J, Huang L, Wang S, Yang F, Ma Y, Xie F, Li L. In vivo immunotoxicity of Gd2 O3 :Eu3+ nanoparticles and the associated molecular mechanism. J Biochem Mol Toxicol. 2020 Nov;34(11):e22562. doi: 10.1002/jbt.22562.
84. Pittenger MF, Discher DE, Péault BM, Phinney DG, Hare JM, Caplan AI. Mesenchymal stem cell perspective: cell biology to clinical progress. NPJ Regen Med. 2019 Dec 2;4:22. doi: 10.1038/s41536-019-0083-6. eCollection 2019. https://doi.org/10.1038/s41536-019-0083-6.
85. Han Y, Yang J, Fang J, Zhou Y, Candi E, Wang J, Hua D, Shao C, Shi Y. The secretion profile of mesenchymal stem cells and potential applications in treating human diseases. Signal Transduct Target Ther. 2022 Mar 21;7(1):92. doi: 10.1038/s41392-022-00932-0. https://doi.org/10.1038/s41392-022-00932-0.
86. Hemmer, E.; Yamano, T.; Kishimoto, H.; Venkatachalam, N.; Hyodo, H.; Soga, K. Cytotoxic Aspects of Gadolinium Oxide Nanostructures for Up-Conversion and NIR Bioimaging. ActaBiomater. 2013, 9, 4734–4743, doi:10.1016/j.actbio.2012.08.045.
87. Dhanalakshmi, S.; Senthil Kumar, P.; Karuthapandian, S.; Muthuraj, V.; Prithivikumaran, N. Design of Gd2O3 Nanorods: A Challenging Photocatalyst for the Degradation of Neurotoxicity Chloramphenicol Drug. J. Mater. Sci. Mater. Electron. 2019, 30, 3744–3752, doi:10.1007/s10854-018-00656-4.